JOURNAL OF GEOPHYSICAL RESEARCH, VOL. 104, NO. E4, PAGES 8489–8507, APRIL 25, 1999

A Mossbauer investigation of iron-rich terrestrial hydrothermal vent systems: Lessons for Mars exploration

Manson L. Wade,[1] David G. Agresti, Thomas J. Wdowiak,
and Lawrence P. Armendarez
Astro and Solar System Physics Program, Department of Physics, University of Alabama at Birmingham

Jack D. Farmer[2]
NASA Ames Research Center, Moffett Field, California

Abstract. Hydrothermal spring systems may well have been present on early Mars and could have served as a habitat for primitive life. The integrated instrument suite of the Athena Rover has, as a component on the robotic arm, a Mossbauer spectrometer. In the context of future Mars exploration we present results of Mossbauer analysis of a suite of samples from an iron-rich thermal spring in the Chocolate Pots area of Yellowstone National **Park** (YNP) and from Obsidian Pool (YNP) and Manitou Springs, Colorado. We have found that Mössbauer spectroscopy can discriminate among the iron-bearing minerals in our samples. Those near the vent and on the surface are identified as ferrihydrite, an amorphous ferric mineraloid. Subsurface samples, collected from cores, which are likely to have undergone inorganic and/or biologically mediated alteration (diagenesis), exhibit spectral signatures that include nontronite (a smectite clay), hematite (α-Fe_2O_3), small-particle/nanophase goethite (α-FeOOH), and siderite ($FeCO_3$). We find for iron minerals that Mossbauer spectroscopy is at least as efficient in identification as X-ray diffraction. This observation is important from an exploration standpoint. **As** a planetary surface instrument, Mossbauer spectroscopy can yield high-quality spectral data without sample preparation (backscatter mode). We have also used field emission scanning electron microscopy (FESEM), in conjunction with energy-dispersive X ray (EDX) fluorescence spectroscopy, to characterize the microbiological component of surface sinters and the relation between the microbiological and the mineralogical framework. Evidence is presented that the minerals found in these deposits can have multi-billion-year residence times and thus may have survived their possible production in a putative early Martian hot spring up to the present day. Examples include the nanophase property and the Mossbauer signature for siderite, which has been identified in a 2.09-billion-year old hematite-rich chert stromatolite. Our research demonstrates that in situ Mossbauer spectroscopy can help determine whether hydrothermal mineral deposits exist on Mars, which is significant for exobiology because of the issue of whether that world ever had conditions conducive to the origin of life. **As** a useful tool for selection of samples suitable for transport to Earth, Mössbauer spectroscopy will not only serve geological interests but will also have potential for exopaleontology.

1. Introduction

During the past two decades since the Viking missions, because of advances in the laboratory tools of molecular biology, our view of phylogenetic relationships among living organisms on Earth has changed dramatically. The universal tree of life, derived from comparisons of genetic sequences found in 16S ribosomal RNA, suggests that life can be subdivided into three major domains: Bacteria, Archaea, and Eukarya *[Woese,* 1987; *Woese et al.,* 19901. These groups appear to have diverged very early in the history of the biosphere from a common thermophilic ancestor *[Barns et al.,* 1996]. **A** number of authors have suggested that terrestrial life may actually have originated at high temperatures *[Corliss et al.,* 1981; *Corliss,* 1990; *Baross and Hoffman,* 1985; *Russell et al.,* 19881. Using thermodynamic models, *Shock and Schulte* [1998, and references therein] have shown that hydrothermal systems are indeed favorable environments for the synthesis of complex organic molecules. Could such hydrothermal systems have provided an environment for the synthesis of prebiotic building blocks for the origin of life on Mars or for the subsequent evolution of Martian life? While a high-temperature origin for terrestrial life is still debatable, the high biological productivity and rapid mineralization that are typical of thermal spring environments make them particularly favorable places for the preservation of a microbial fossil record. For this reason, hydrothermal deposits are re-

[1]Also at Russell Mathematics and Science Center, Alabama School of Fine Arts, Birmingham.
[2]Now at the Department of Geology, Arizona State University, Tempe.

Paper number 1998JE900049.
0148-0227/99/1998JE900049$09.00

garded as important targets in the exploration for fossil evidence of ancient Martian life [*Farmer,* 1995; *Farmer and Des Marais,* 1994; *National Aeronautics and Space Administration (NASA),* 1995; *Walter and Des Marais,* 1993].

Much of the surface of Mars is covered by deposits of fine-grained materials consisting of nanophase and macroscopic (or "bulk") crystalline iron oxides, silicate mineraloids, and salts, as studied by *Geissler et al.* [19931, *Banin et al.* [19971, *Mustard and Hays* [1997], *Morris et al.* [1997], and *Morris and Golden* [1998]. These authors have suggested that the elemental composition of the soils at the Viking and Pathfinder sites can be explained as the by-product of recent weathering of mafic volcanic rocks in the presence of acidic volatiles produced during periodic episodes of volcanism. The lack of surface water during the younger epochs of Martian history, along with low temperatures, is likely to have halted the transformation of metastable amorphous mineraloids to more ordered, crystalline mineral phases. In many places, thick deposits of such materials may overlie older deposits of aqueous sediments formed during the warmer, wetter period in Martian history.

Could hydrothermal systems have been common on Mars during this earlier period? On Earth, subaerial hydrothermal springs are common features of continental volcanic settings [*Pirajno*, 19921. Photogeologic evidence suggests that volcanic terrains are also widespread on Mars [*Mouginis-Mark et al.,* 19921. The higher heat flow, widespread volcanism, and likelihood of occasional large impacts during the latter part of heavy bombardment suggest that hydrothermal systems may have been also widespread on early Mars [*Sleep and Zahnle,* 19981. Indeed, in the ancient, heavily cratered terrains of Mars, there are many examples of channels associated with potential heat sources such as large impact craters, volcanic cones, or chaotic features which suggest the possibility of ancient hydrothermal systems [*Farmer,* 19961. Surface hydrological systems appear to have been active during late heavy bombardment at a time when sizeable impacts were still occurring [*Carr,* 19961. While impact-related metamorphism and brecciation of the surface materials may have partially overprinted some of the earliest record of aqueous environments, associated hydrothermal systems were probably also widespread and are likely to have contributed significantly to the inventory of early aqueous sedimentary deposits at and near the surface [*Brakenridge et al.,* 1985; *Newsom,* 1980; *Farmer,* 19961.

Newsom [19971 suggested that hydrothermal systems on Mars may have evolved from water-dominated (neutral chloride surface springs) to vapor-dominated (fumerolic) systems as the planet lost its atmosphere and surface water dried up. In vapor-dominated systems the sulfur/chlorine ratio tends to be high (>>1.0), while in neutral chloride and alkaline springs the ratio of sulfur/chlorine is low (<1.0). The elemental abundance data for the Viking and Pathfinder sites (thought to be younger Martian terrains) do show sulfur/chlorine ratios of ~11 at the Viking 2 site and ~4 at Viking 1 and the Pathfinder sites, which is consistent with vapor-dominated hydrothermal processes. If widespread hydrothermal systems became progressively vapor-dominated over time, this should be detectable by comparing differences in surface mineralogy for different aged terrains.

A decade ago, we and others recognized the utility of miniature Mossbauer spectrometers as in situ instruments for landed spacecraft [*Morris et al.,* 1988, 1989a; *Shelfer,* 1992; *Knudsen*, 1989; *Knudsen et al.*, 1990, 1991; *Evlanov et al.,* 1991; *Klingelhofer et al.,* 19921 and furthermore that in addition to conventional mineralogy, Mossbauer spectroscopy has a role to play in exobiological investigations [*Agresti and Wdowiak,* 1992; *Agresti et al.,* 1994; *Wdowiak et al.,* 19951. Deposits of putative Martian hydrothermal environments would likely be rich in iron, making them amenable to Mossbauer spectroscopy. In fact, a Mossbauer spectrometer, employing the 14.4-keV resonance in ^{57}Fe and functioning in the backscatter mode [*Klingelhofer et al.,* 1994; S.W. Squyres, http://astrosun.tn.cornell.edu/athena/mossbauer. html, 1998a], is a planned component of the Athena rover instrument suite [*Squyres et al.,* 1998; S.W. Squyres, http://astrosun.tn.cornell.edu/athena/instruments.html, 1998b] to be launched to Mars in 2003 as part of NASA's restructured Mars exploration program. This instrument is also included as part of the planned Athena Precursor Experiment (APEX) on the 2001 Lander, to be mounted on its robotic arm (S.W. Squyres, http://astrosun.tn.cornell.edu/athena/xinstruments.html, 1998c). Among the stated capabilities of the Mossbauer instrument is the ability to detect "nanophase and amorphous hydrothermal Fe minerals that could preserve biological materials" (S.W. Squyres, http://astrosun.tn.cornell.edu/athena/mossbauer.html1998a).

Terrestrial hydrothermal springs, including deep-sea vents, harbor complex ecosystems that have evolved based on nutrients and energy supplied by the vent effluent. Importantly, land-based spring systems also include photosynthetic (cyanobacterial) species. Previously, we reported results of a Mossbauer investigation of samples (collected by J. C. Alt) from submarine hydrothermal vents ("black smokers") in an area of the East Pacific Rise [*Agresti et al.*, 19941. The iron-rich minerals were shown by scanning electron microscopy (SEM) to be associated with bacterial filaments [*Alt,* 19881. Mossbauer spectra taken over a range of sample temperatures revealed that the material collected at active vents is amorphous. Once the vents become inactive, the organic component of encrusted filaments is lost, leaving behind filament molds, while the primary amorphous materials undergo recrystallization to ordered phases. We found that this fossilizing medium is nanophase (superparamagnetic) material.

In this paper we report on a study of iron-bearing phases in several iron-oxide depositing subaerial hydrothermal springs. Samples we investigated were collected at Manitou Springs, Colorado, and in Yellowstone National Park (YNP). The primary analytical technique employed was transmission iron Mossbauer spectroscopy, carried out over a range of cryogenic temperatures, supplemented by powder X-ray diffraction (XRD), field emission scanning electron microscopy (FESEM), and energy dispersive X-ray (EDX) fluorescence spectroscopy. Previously [*Agresti et al.,* 19951, we reported a rich variety of Mossbauer spectral signatures exhibited by samples collected from an iron-rich hydrothermal mound at East Chocolate Pots, Yellowstone National Park. Here we focus on a suite of samples collected systematically along an outflow channel of this mound; a preliminary report was prepared by *Agresti et al.* [19971.

We also discuss evidence that the Mossbauer signatures of hydrothermal deposits can survive for billions of years. In this context, we will compare Mossbauer and Raman spectroscopic measurements made on a 2.09-billion-year old hematic chert stromatolite. Our results support the utility of Mossbauer spectroscopy as an in situ instrument that can prospect for ancient hydrothermal deposits on Mars. It has the poten-

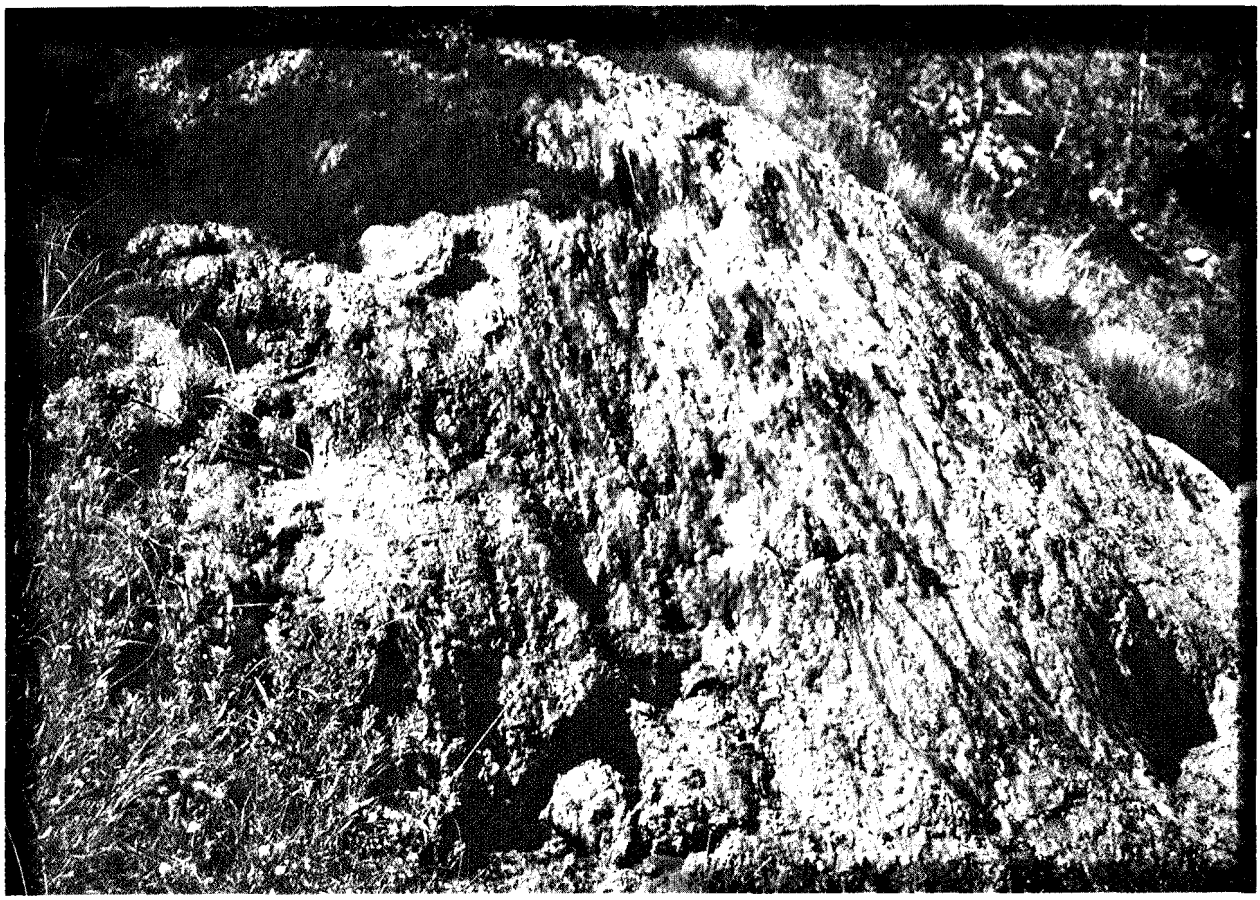

Plate 1. A close-up view of the active iron-rich vent mound at the Chocolate Pots, Yellowstone National Park (YNP), from which samples studied in this work were collected. Bacterial streamers can be seen along the front face of the mound while the outflow channel lies just beyond the right of the image. A photograph of the entire mound was published previously [*Agresti*, 1995]. Note the contrast in color of this east bank mound and that described by *Allan and Day* [1935].

tial to identify exobiologically relevant samples for delivery to Earth as part of the planned sample return starting with the 2005 Mars Surveyor mission, in which it is likely that the Athena Rover will be the collection platform.

2. Samples and Methods

2.1. Samples

Samples evaluated in this report were obtained from several hydrothermal settings. Initial discussion pertains to two samples collected from an iron-rich outflow stream at Manitou Springs, Colorado, and along the margins of Obsidian Pool (formerly Jim's Black Pool) in Yellowstone National Park (YNP), Wyoming, where several small iron-oxide depositing thermal springs exist (see *Barns et al.* [1996] for a discussion of Obsidian Pool).

Collection was done also at the Chocolate Pots (YNP), along the shallow, main outflow channel of a large, iron-rich thermal spring mound (Plate 1) on the east bank of the Gibbon River, which is ~8 m below the vent. The area has been infrequently described in the literature (L. Whittlesey, YNP, Archivist and Historian, personal communication, 1999). *Erwin* [1898, p. 15] mentions "two beautiful chocolate-colored geysers situated on opposite sides of the Gibbon River" that are "immense cones." *Allen and Day* [1935, pp. 357-3591 provide more extensive discussion, including analyses of effluent water and ferruginous sinter, and a photograph of the conical mound prominent on the west bank of the river. They describe the most "striking characteristic" to be the "color, rich brown with streaks of black." *Whittlesley* [1988, pp. 277-278] discusses the origin of the name of the site.

At the Chocolate Pots we obtained a suite of 13 samples at four locations (Table 1) along the outflow channel. Properties of the water (temperature T hydrogen ion concentration pH; and redox potential Eh) in the channel above each collection site were measured (Table 1 and Figure 1). Each site was cored to a depth of at least 1 cm by pressing a I-cm-diameter tube into the sediment, except at the vent, where materials were too friable. Cores were then subdivided into depth intervals (as in Table 1) using a razor blade. Immediately following field collection, samples were preserved for transport at about -5°C to inhibit further chemical change, and then stored at about -25°C in the laboratory. Upon drying, samples collected near the stream (2C1-2C4, 3C1-3C4) all formed a fine powder. However, material collected closer to the vent (5C1-4, 6C1) formed a glassy, laminated material. A microscope (20X) shows this material to consist of thin (~50 μm) alternating light and dark (reddish) bands. It fractures readily on handling and was easily pulverized with a mortar and pes-

Table 1. Chocolate Pots Mossbauer Samples

	Distance Below Vent, m			
Depth, mm	7	6	2	0
0-1	2C1	3C1	5C1	
1-4	2C2	3C2	5C2	
4-8	2C3	3C3	5C3	
>8	2C4	3C4	5C4	
0-10				6C1
T, °C	48.0	53.2	54.2	55.0
pH	1.9	7.8	1.2	5.8
Eh, mV	-49.0	-45.1	-2.0	81.7

Thirteen samples from East Chocolate Pots (YNP), taken at four locations along the main outflow channel, measured from the vent, and cored to four depths, as indicated. Included also are temperature T, hydrogen ion concentration pH, and redox potential Eh, of the water immediately above the collection site.

tle. For Mossbauer analysis the powdered samples were dispersed in molten (~55°C) paraffin, then quickly pressed into a 1.6-cm-diameter pellet, typically containing ~20 mg of sample/cm^2.

Duplicate cores were collected at each of the Mossbauer sample sites, and the upper mm (2C1, 3C1, 5C1, Table 1) was examined by field emission scanning electron microscopy (FESEM) and energy dispersive X-ray (EDX) fluorescence spectroscopy to characterize the nature of the microbial community and the primary precipitates. An additional sample (7C1) was collected from a steep part of the mound surface located just below first break in the slope, which was covered with microterracettes; this site was in an area of very shallow sheet flow, and measurements of temperature, pH, and Eh were not possible. To preserve the structure of the organisms present, samples were fixed in the field using a mixture of 2% glutyraldehyde and 4% formalin in filtered spring water. Upon returning to the laboratory the upper few millimeters were subsampled from cores, fixatives removed and samples dehydrated by passing them through a graded ethanol series (10-25-50-75-95-100-100%). Samples were stored in 100% ethanol and later critical point dried (CPD) using a Pelco model CPD-2 critical point dryer. Further description of these samples will be discussed in section 3.6.

One additional sample, a 2.09-billion-year old (Ga) hematite-rich chert stromatolite from the Gunflint Iron Formation, southern Ontario (Nolalu), Precambrian Paleobiology Research Group (PPRG) sample 2443 (provided by J.W. Schopf, University of California, Los Angeles), is discussed in this work. Certain of its spectral features are similar to those of some of the Chocolate Pots samples. A slab, ~70 μm in thickness by ~1 cm^2, was freshly cut from a solid mass for Mossbauer investigation.

2.2. Instrumentation

The Mossbauer spectrometer operates in transmission geometry in constant-acceleration mode. Velocity calibration is done with reference to standard Mossbauer materials, principally hematite, a-iron metal, and sodium nitroprusside. The activity of the ^{57}Co source (270-day half-life) ranged from 50 to ~20 mCi, depending on length of time since its delivery. Mossbauer measurements, at temperatures from 300 K to 12 K, employed an APD Cryogenics "Displex" 202 closed-cycle refrigerator, with two-stage expander, coupled by gaseous helium to the APD Cryogenics vibration-isolated Mossbauer shroud, and a Lakeshore 330 temperature controller.

The X-ray powder diffraction analysis was carried out using a Siemens D500 diffractometer. Interplanar spacings ("d" values) were computed using the copper K_α X-ray wavelength (λ = 0.1542 nm) and the Bragg formula. Mineral identification was based on standard powder diffraction files *[Joint Committee on Powder Diffraction Standards (JCPDS),* 1980]. Estimates of mean particle size t were made using the Scherrer formula [*Cullity,* 1978, equation (3.13)]

$$t \approx \frac{0.9\lambda}{B\cos\theta_B} \quad (1)$$

where B (in radians) is the line broadening (of the full width at half maximum, FWHM) due to small particle effects, obtained in quadrature with reference to an unbroadened line, and $\theta_B = \frac{1}{2}(2\theta)$ is the Bragg angle of the line.

FESEM and EDX data were acquired after mounting samples on SEM stubs with silver paint and coating with 4.0 nm of iridium using an ion beam sputter coater (VCR IBM Model TM2005). Coated samples were examined with a Hitachi S-4000 cold field emission SEM having an image resolution of 1.5 nm. Samples were examined at 15 kV; selected areas were also analyzed and elemental compositions identified using a Noran/Voyager, EDX microanalysis system.

2.3. Mossbauer Analysis

Spectral data were least squares fit with a sum-of-Lorentzians model based on the standard hyperfine interactions appropriate for Mossbauer spectroscopy *[Agresti et al.,* 1969; *Bent et al.,* 19691. For each distinct atomic site (nuclear environment) the adjustable parameters were isomer shift, IS (relative to a-iron metal); electric quadrupole hyperfine splitting or shift (see below), QS; effective magnetic hyperfine field at the nucleus, B_{hf}; Lorentzian line width, W (full width at half maximum); and relative spectral area, Area. Each spectrum was modeled as a superposition of individual doublet (B_{hf} = 0) or sextet components ($B_{hf} \neq 0$). Parameter

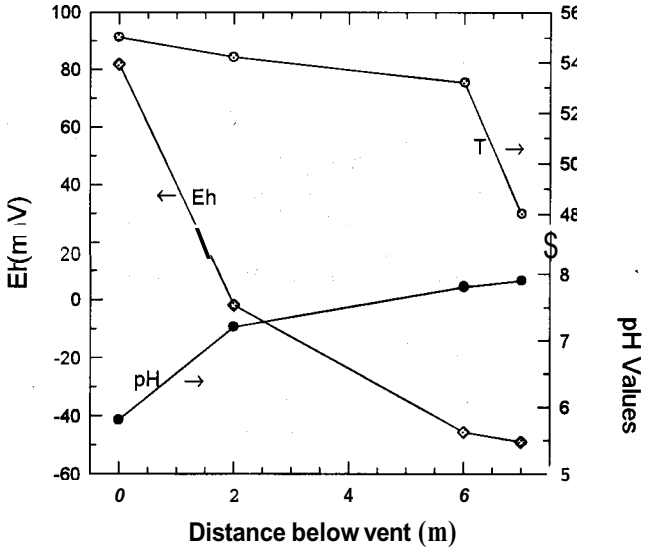

Figure 1. Plot of temperature T, hydrogen ion concentration pH, and redox potential Eh versus distance below the vent.

standard deviations were generally less than 0.02 mm/s for IS and QS; 0.01 mm/s for W; 0.1 T for B_{hf}; and 0.5% for Area. Superposition spectra come about either because of nonequivalent atomic environments within a single mineral phase or because of the presence of several iron-bearing phases. For a doublet component the two peaks are assigned equal areas, while sextet components are modeled with peak areas in the ratio, 3:2:1:1:2:3, generally appropriate for powdered (nonoriented) samples.

A range of measurement temperatures was employed, not only to investigate Mars analogue materials at Mars ambient temperatures but also to enhance information yield. Parameters generally vary with temperature in a characteristic way, and there may also be a phase change (e.g., magnetic ordering) as temperature is lowered. The first is typically a subtle effect, while the latter can dramatically alter the appearance of the spectrum. Several examples appear in this work of spectra whose components overlap at certain temperatures but are well separated at others. The "typical" standard deviations listed above refer to spectra with reduced overlap, which results in smaller correlations among parameter values (especially W and Area, which, conversely, are less reliable when overlap is strong) and a reduction in ambiguity of assignments, with a corresponding increase in the reliability of the inferred mineralogy.

Spectral analysis can resolve the valence of iron and the degree of magnetic order in a mineral phase. A doublet (or singlet) component arises when the magnetic interaction averages to zero ($B_{hf} = 0$); in this case, the doublet peak separation is known as the "quadrupole splitting" and may be designated QS. When the material is magnetically ordered and $B_{hf} \neq 0$, the situation is more complicated. Here the effect of a quadrupole interaction is to shift the inner quartet (2:1:1:2) and the two outer lines (3:3) of the sextet in relation to each other in a way that keeps the center of gravity (IS) constant. This shift is called the "quadrupole shift" and for simplicity will be designated here also with QS, since the two effects are readily distinguished according to whether $B_{hf} = 0$ or not. Quadrupole splitting ($\Delta = 0$) and quadrupole shift ($B_{hf} \neq 0$) are not identical (see, e.g., Tables 2, 3, and 5), since in addition to the underlying electric quadrupole interaction the quadrupole shift is affected by the relative orientation of the magnetic hyperfine field and the principal axis of the electric field gradient tensor (see *Wegener* [1965] for an exceptionally thorough discussion of this topic). When the quadrupole splitting is small, ferric iron (Fe^{3+}) is usually indicated (Figure 2, 300 K). A more widely spaced doublet suggests ferrous iron (Fe^{2+}) (see, e.g., Figure 7, 2C3). When quadrupole splitting, and hence quadrupole shift, is large, the peaks of the magnetic sextet may be reordered (as in Figure 16, where the order is 2:3:1:1:2:3). The precise values of the principal spectral parameters, IS, QS, and Δ thus serve as a fingerprint in identifying the particular mineral phase or compound [see, e.g., *Bancroft,* 1973; *Mitra,* 1992; *McCammon*, 19951.

For well-crystallized material the typical measured peak width W is ~0.3 mm/s. In this study we have also observed broadened lines, which may be attributed to (1) an amorphous nature of the material; (2) a collection of similar crystallites with variable bulk properties, such as particle size, as for the nanophase material found in this work; and (3) dynamical effects, such as "collective magnetic excitations" [*Mørup and Topsoe*, 1976; *Mørup*, 1983]. Broadened doublet spectra (see Figure 10) are modeled as a superposition of two sites, with variable quadrupole splitting QS and width W along with a common isomer shift IS. Broadened sextet spectra are generally also skewed (Figure 2, 12 K) in a way that preserves the mirror symmetry of peak pairs (1,6; 2,5; 3,4). Peak broadening results from a distribution of magnetic hyperfine fields and thus can be shown to increase linearly from center outward, so that a single broadening parameter A accounts for this ($W_{3,4}=W; W_{2,5}=W+\frac{1}{2}\Delta; W_{1,6}=W+\Delta$). Similarly, asymmetry in the field distribution, which is characteristic of nanophase particles, leads to asymmetry in the shape of individual sextet peaks. We have found [e.g., ***Morris et al.,*** 1989b] that this effect can be adequately modeled with a single skew parameter κ by joining two half Lorentzians at their midline (outer half width is $\frac{1}{2}W_i/\kappa$; inner half width is $\frac{1}{2}W_i \times \kappa$; where $\kappa > 1$ and $i = 1$ to 6). While these two added parameters improve the fit and thus add to the reliability of the model, their precise values do not affect the interpretation of results presented in this work and will not be reported here.

In the particular case of material exhibiting superparamagnetic behavior [*Kündig et al.,* 1966] the spectrum typically consists of a doublet plus a sextet component, where the doublet intensity decreases as temperature is lowered, while the

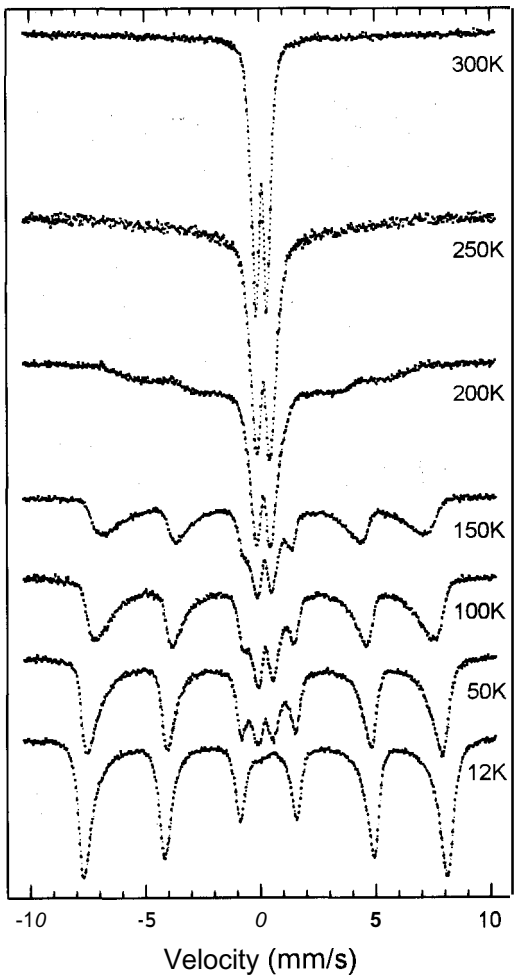

Figure 2. Mossbauer spectra for the sample from Manitou Springs, Colorado, acquired over a range of temperatures, as indicated.

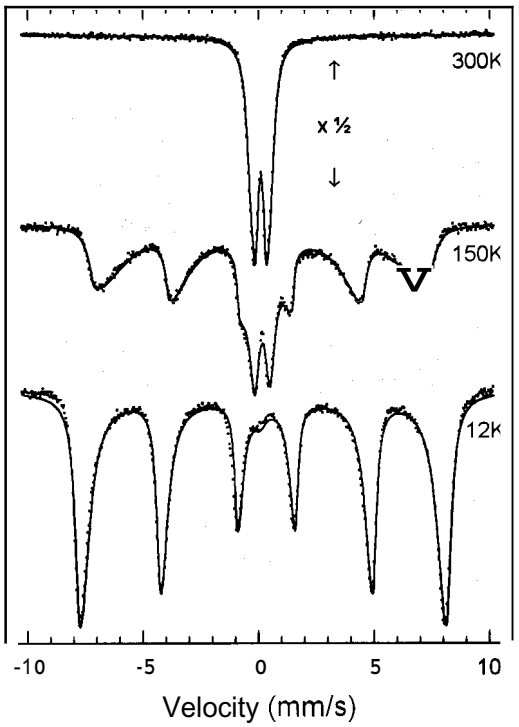

Figure 3. Representative least squares fits (solid lines) of Manitou Springs spectra. The **300** K spectrum is modeled as a doublet (sum of two Lorentzians). The 12 K spectrum is fit with a broadened and skewed sextet, while the 150 K spectrum is a superposition of these two models

Table 2. Manitou Springs Mossbauer Parameters

Temperature, K	IS, mm/s	QS, mm/s	B_{hf}, T	W, mm/s	Area, %
300	0.25	0.48	--	0.35	58.0
	0.25	0.89	--	0.42	42.0
250	0.29	0.55	--	0.46	36.5
	0.25	-0.08	19.7	0.38	63.5
225	0.30	0.67	--	0.56	35.8
	0.32	-0.22	34.2	0.80	64.2
200	0.30	0.69	--	0.57	26.2
	0.35	-0.23	38.9	0.68	73.8
150	0.31	0.68	--	0.53	21.0
	0.37	-0.20	44.4	0.50	79.0
100	0.35	0.69	--	0.54	19.4
	0.41	-0.18	46.2	0.49	80.6
50	0.36	0.69	--	0.63	17.0
	0.41	-0.18	48.1	0.44	83.0
12	0.42	-0.15	49.2	0.43	100
bGt, 22 K	0.47	-0.25	49.8	--	--

Fits modeled as a superposition of a doublet ($B_{hf} = 0$), appropriate for nanophase (np) goethite above the superparamagnetic blocking temperature (T_B), plus a broadened and skewed sextet ($B_{hf} \neq 0$), due to goethite below T_B. For improved fit a pair of doublets is used at 300 K. **Also** included are reference values for **bulk** goethite (bGt) at 22 K *[Morris et. al.*, 1989b].

those of bulk goethite (α-FeOOH). We conclude that the iron-bearing phase of the Manitou Springs sample is nanophase goethite.

Spectra of the sample taken from Obsidian Pool (YNP) (Figure 4) are somewhat more complex. The doublet-to-sextet conversion, indicative of superparamagnetism, is still

sextet area correspondingly increases (Figure *2).* Even though the material is below its magnetic ordering temperature (where neighboring atomic moments are correlated), for sufficiently small (~10-100 nm; hence "nanophase") particles, thermal effects may overwhelm the tendency of the moments to orient in a particular crystalline direction (the "easy axis"). This tendency to orient and, most importantly, to result in a nonzero value of B_{hf} is proportional to particle volume [*Kündig et al.,* 19661. Thus a sextet pattern is achieved for small particles only below the so-called "blocking" temperature, at which the doublet-to-sextet conversion takes place. The range of temperatures over which doublet and sextet coexist indicates a distribution of particle sizes, the smaller particles (at a given temperature) being associated with the doublet, the larger particles with the sextet. This behavior is a signature for "superparamagnetism."

3. Results and Discussion

3.1. Manitou Springs and Obsidian Pool

Figure 2 shows a Mossbauer temperature sequence for the sample from Manitou Springs, Colorado. Fits of three spectra of differing degrees of complexity are shown in Figure 3. To fit the 300 K spectrum, a pair of doublets is used, whereas the 12 K spectrum is fit with a broadened and skewed sextet. The intermediate spectrum (150 **K)** includes both the doublet and sextet components just discussed. The results (Table 2) show that as temperature is lowered, the area of the doublet gradually decreases, while the sextet area increases, a characteristic of superparamagnetic behavior, while the values determined for the hyperfine parameters at low temperatures tend toward

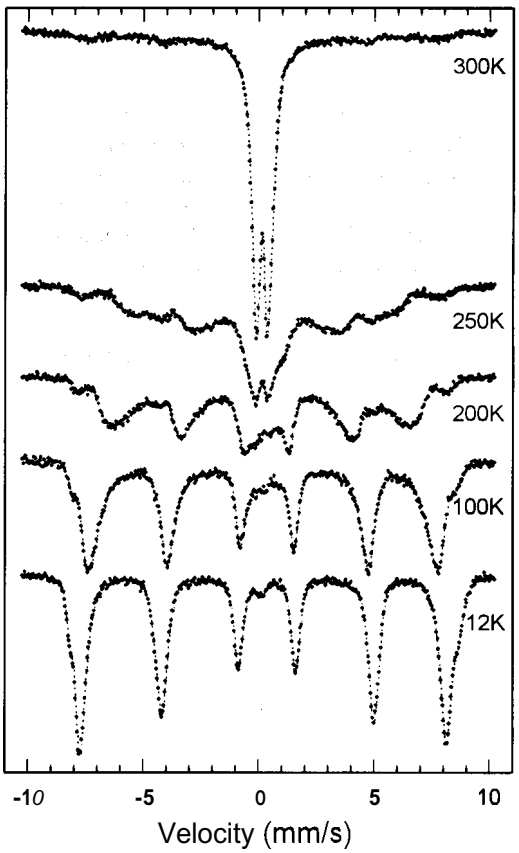

Figure 4. Mossbauer spectra of the sample from Obsidian Pool (YNP), acquired over a range of temperatures, as indicated.

Table 3. Obsidian Pool Mossbauer Parameters

Temperature, K	IS, mm/s	QS, mm/s	B_{hf}, T	W, mm/s	Area, %
300	0.24	0.55	--	0.46	89.7
	0.26	-0.16	46.9	2.32	10.3
250	0.28	0.60	--	0.57	14.3
	0.31	-0.21	34.9	0.71	79.1
	0.33	-0.19	48.3	0.70	6.6
200	0.25	0.57	--	1.04	9.5
	0.34	-0.23	40.9	0.56	85.2
	0.34	-0.12	49.7	0.47	5.3
100	0.40	-0.19	47.1	0.43	92.4
	0.39	-0.07	51.5	0.30	4.4
12	0.42	-0.19	49.2	0.40	75.6
	0.43	-0.05	51.8	0.34	22.7
bGt, 22 K	0.47	-0.25	49.8	--	--
nHm, 22 K	0.48	-0.08	50.0	--	--

Fits modeled as in Table 2, with an additional sextet component due to nanophase (np) hematite. Included also are reference **values** for bulk goethite (bGt) and np hematite (nHm) at 22 K (sample S6FN21 of *Morris et. al.* [1989b]).

observed but takes place **over** a narrower temperature range, and an additional, more widely spaced sextet component, with smaller line widths, appears. Values of the fitted parameters are given in Table *3,* with an analysis of the 250 K spectrum shown in Figure 5. As for Manitou Springs, the dominant phase is nanophase goethite. The new spectral component is consistent with nanophase hematite (α-Fe_2O_3).

Figure 6 shows the variation with temperature of the magnetic hyperfine field, B_{hf}, for the sextet components of the samples from Manitou Springs and Obsidian Pool, along with the variation for bulk goethite [*Mørup*, 1983]. The upper curve in Figure 6 lies well above the others, as expected for hematite (T_N>>300 K). The curves for the nanophase goethite components of the two samples are quite similar, with apparent ordering temperature T_p of ~275 K, well below that of bulk goethite (T_N = 393 **K)** [*Coey*, 19881. We note that the

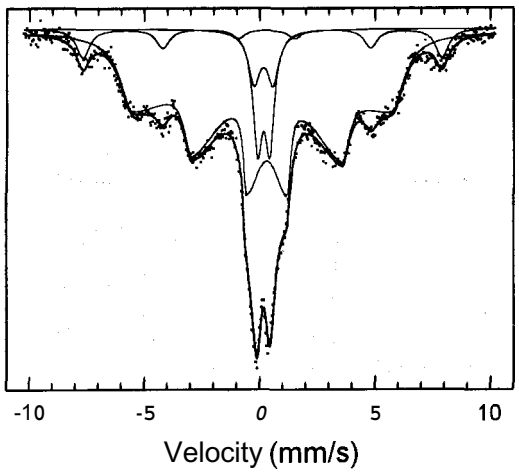

Figure 5. Least squares fit of the 250 **K** spectrum for Obsidian Pool. The full fit is shown as the dark line through the data. The component spectra (lighter lines) include a widely spaced sextet due to nanophase (np) hematite, a broadened and skewed sextet with smaller overall splitting (np goethite above its blocking temperature), and a pair of overlapping doublets (np goethite below its blocking temperature).

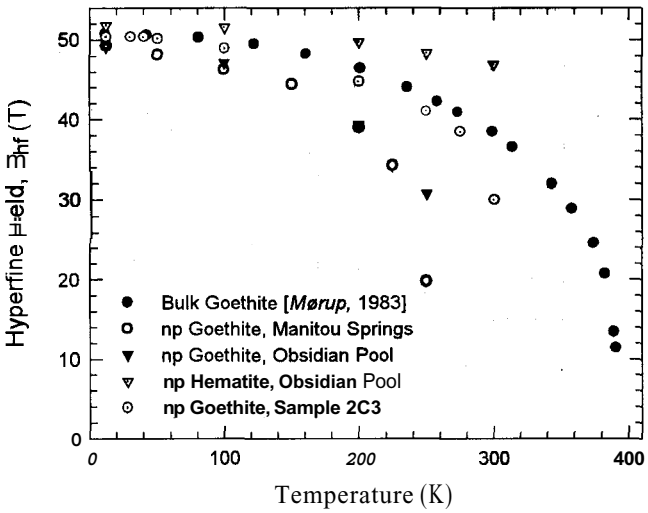

Figure 6. Variation of the magnetic hyperfine field B_{hf} with temperature for several phases derived from fits to the Manitou Springs and Obsidian Pool spectra, along with bulk goethite [*Mørup*, 19831. Also shown is similar plot for the nanophase (np) goethite component of sample 2C3 (discussed in section 3.4.1).

goethite in sample 2C3 (see below) has a value of T_p intermediate between that of bulk goethite and the samples from Manitou Springs and Obsidian Pool. *Koch et al.* [1985] give several examples illustrating the range of variation of T_p for various samples of goethite.

3.2. Chocolate Pots (YNP) Room Temperature Mossbauer Spectra

The **300** K spectra (Figures 7-9) were acquired for all 13 samples listed in Table 1. They fall into two distinct catego-

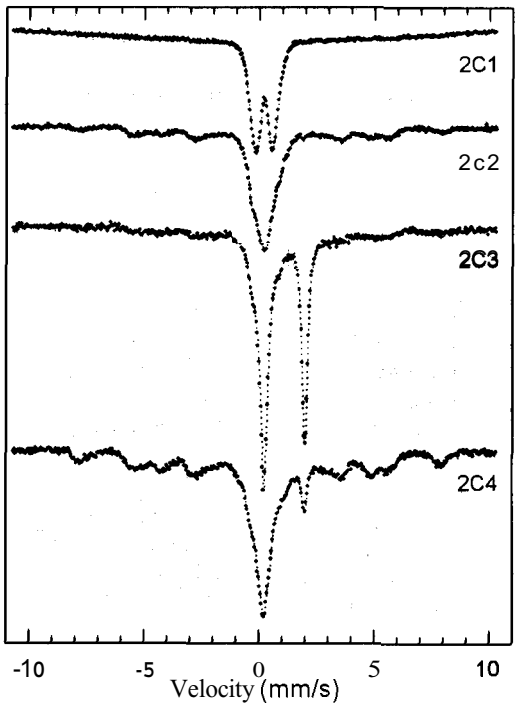

Figure 7. The 300 K Mössbauer spectra of core samples 2C1-4 (collected 7 m below the vent).

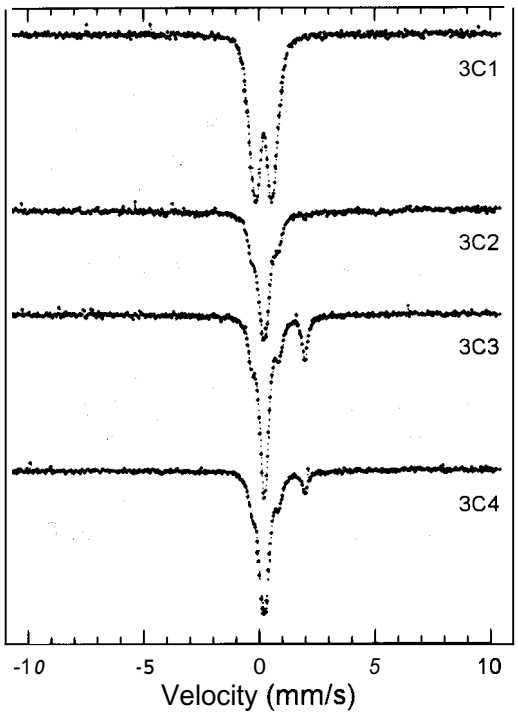

Figure 8. The 300 K Mossbauer spectra of core samples 3C1-4 (collected 6 m below the vent).

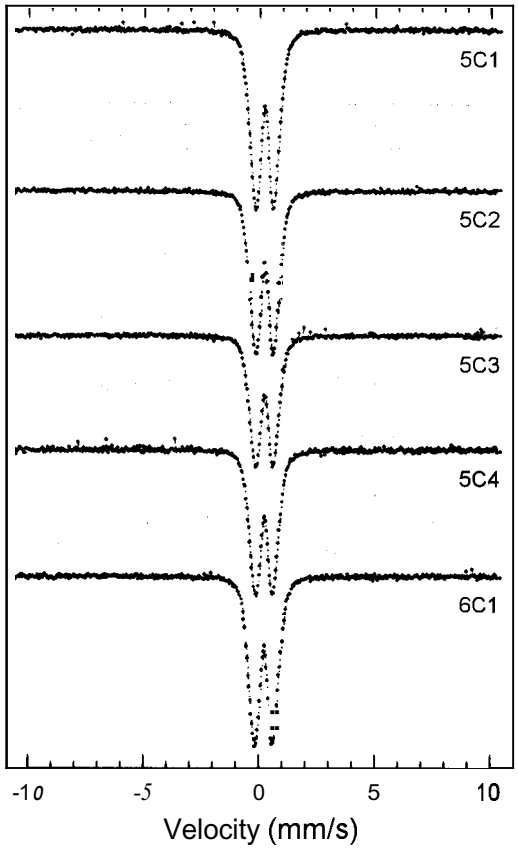

Figure 9. The 300 K Mossbauer spectra of core samples 5C1-4 and 6C1 (collected near the vent).

ries: (1) broad ferric doublets (surface samples and those near the vent, 2C1, 3C1, 5C1-4, 6C1); and (2) more complex spectra (samples at depth nearer the river, 2C2-4, 3C2-4). Intuitively, these two categories correspond to samples that can be considered primary precipitates (at the surface or near the vent) and the "subsurface" samples, which would have had the opportunity to undergo diagenetic change. A similar distinction was made previously for the deep-sea vent samples [*Agresti et al.*, 19941, where samples from active vents were contrasted with those from inactive vents.

3.3. Primary Precipitates ("Surface" Samples)

The broad ferric doublets characteristic of the seven "surface" samples were modeled in two ways, as a single doublet and as a pair of overlapping doublets with common isomer shift. Representative fits (for 6C1 and 2C1) are shown in Figure 10. Note that the 6C1 fit is improved with the two-site model; the 5C1-4 and 3C1 spectra, not shown, are very similar. However, the model fails to fit the background for 2C1, suggesting a contribution from a weak magnetic component with transition temperature near 300 K. The results of the fits to the 300 K spectra of the seven "surface" samples are presented in Table 4, along with reported parameter values for ferrihydrite (formula varies, e.g., ~$Fe_5HO_8 \cdot 4H_2O$ [*Murad*, 1988] or $5Fe_2O_3 \cdot 9H_2O$ [*Coey*, 19881). A close agreement is seen to exist between these values (IS, QS, and *W*) and those measured for the seven "surface" samples.

Spectra of the 6C1 sample, taken over a range of temperatures, are similar to those of the 5C1-4 core samples and are shown in Figure 11. At 14 K the peaks are still broad (a result of the amorphous nature of the samples), and a single broadened, skewed sextet model results in an adequate fit. The parameters, IS, QS, B_{hf}, and *W* (Table *5)* are all consistent with

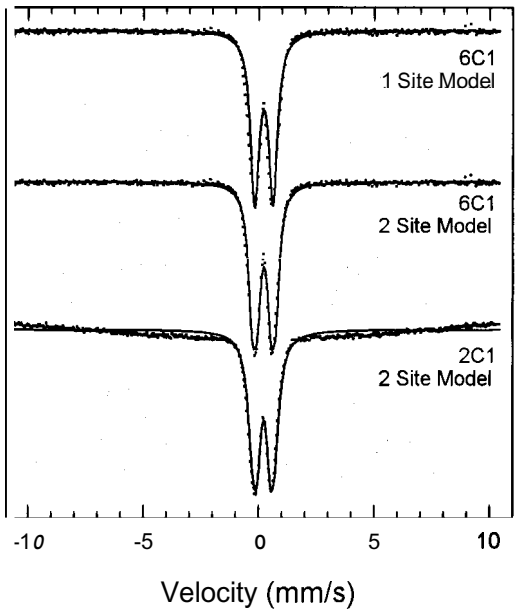

Figure 10. Representative fits (solid lines) for the 300 K spectra of the "surface" samples, 6C1 and 2C1. The 6C1 spectrum is modeled as a single, broadened doublet (one-site model) and as a pair of broadened doublets (two-site model). Note the sloping background in the 2C1 spectrum, which implies an additional contribution from a broadened magnetic sextet.

Table 4. "Surface" Mossbauer Parameters at 300 K

Sample	IS, mm/s	QS, mm/s	W, mm/s	Area, %
2c1	0.35	1.07	0.38	36.2
	0.35	0.61	0.40	64.8
3C1	0.33	1.06	0.38	36.4
	0.33	0.59	0.42	64.6
5C1	0.34	1.08	0.42	48.8
	0.34	0.63	0.36	51.2
5C2	0.34	1.08	0.42	48.2
	0.34	0.63	0.37	51.8
5c3	0.35	1.10	0.39	39.3
	0.35	0.64	0.38	60.7
5c4	0.35	1.03	0.42	39.6
	0.35	0.58	0.35	60.4
6C1	0.35	0.80	0.45	100
6C1	0.35	1.09	0.41	46.0
	0.35	0.63	0.36	54.0
Feh	0.35	0.7-0.85	>0.4	--
Feh	0.35	−0.90	−0.4	--
	0.35	−0.50	−0.4	--

Fits modeled as a superposition of two doublets with common isomer shift (plus a one-doublet fit for 6C1). Included also are reference fit results for ferrihydrite (Feh) *[Murud,* 19881.

Table 5. Sample 6C1 Mössbauer Parameters

Temperature, K	IS, mm/s	QS, mm/s	B_{hf}, T	W, mm/s	Area, %
300	0.35	1.08	--	0.41	46.0
	0.35	0.63	--	0.36	54.0
100	0.46	1.11	--	0.44	49.2
	0.46	0.63	--	0.36	50.8
50	0.44	1.16	--	0.48	45.0
	0.44	0.65	--	0.42	55.0
45	0.47	0.95	--	0.83	92.5
	0.47	0.61	--	0.31	7.5
30	0.48	-0.07	38.1	1.06	100
25	0.47	-0.06	41.4	0.97	100
20	0.47	-0.05	44.0	0.89	100
14	0.47	-0.06	46.0	0.73	100
Feh, 4.2 K	0.46	-0.02 - -0.10	46.5 - 50.0	1.7 - 0.9	--

For higher temperatures, fits modeled as in Table 4. At lower temperatures, fits modeled with a broadened and skewed sextet. Included also are reference values for ferrihydrite (Feh) at 4.2 K *[Murud,* 19881, where widths are given for the outer lines and ranges are given for "2-" to "6-XRD-line" ferrihydrites, respectively. For sample 6C1 at 14 K, outer line widths are −1.4 mm/s.

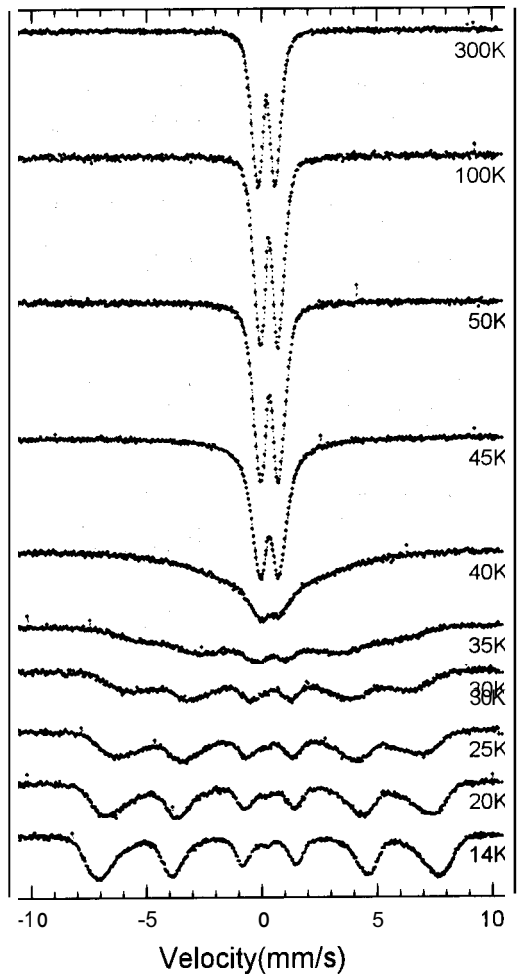

Figure 11. Mossbauer spectra for sample 6C1, taken at various temperatures.

those reported for ferrihydrite at 4.2 K *[Murud,* 1988]. The Néel temperature, T_N −45 K (Figure 11), is within the range (<78 K) typical of ferrihydrite, whose ordering temperature is reduced for poorer crystallinity *[Murud and Bowen,* 19851. Taken together with the 300 K results, we may conclude that the iron-bearing phase in the 6C1 and 5C1-4 samples is ferrihydrite.

The situation regarding the 2C1 and 3C1 samples is less clear. While the 300 K data are consistent with ferrihydrite, no associated magnetic transition is observed down to 13 K. The fit results (Table 6), including the low-temperature data, demonstrate that the weak magnetic component seen at 300 K in the 2C1 spectrum is due to goethite, which is often found associated with ferrihydrite in watery environments [*Schwertmann,* 19881.

X-ray powder diffraction patterns were obtained for the seven "surface" samples (Figure 12). These poorly crystalline samples exhibit very broad bands, as expected. Of course, clear identification from the diffraction pattern is not possible for amorphous material. However, the patterns for the "sur-

Table 6. Sample 2C1 Mossbauer Parameters

Temperature, K	IS, mm/s	QS, mm/s	B_{hf}, T	W, mm/s	Area, %
300	0.35	1.05	--	0.57	66.5
	0.35	0.60	--	0.42	16.1
	0.46	-0.33	29.5	3.50	17.4
200	0.41	0.95	--	0.56	39.0
	0.41	0.54	--	0.33	13.3
	0.46	-0.29	35.1	3.00	47.7
25	0.67	0.83	--	0.36	21.3
	0.40	0.79	--	0.53	68.5
	0.48	-0.28	50.1	0.49	10.2
13	0.44	0.73	--	1.09	88.6
	0.46	-0.27	50.2	0.29	11.4
bGt, 22 K	0.47	-0.25	49.8	--	--

Fits modeled as a superposition of two doublets and a sextet at higher temperatures and a doublet plus sextet at 13 K. Included also are reference values for bulk goethite (bGt) at 22 K *[Morris et al.,* 1989b].

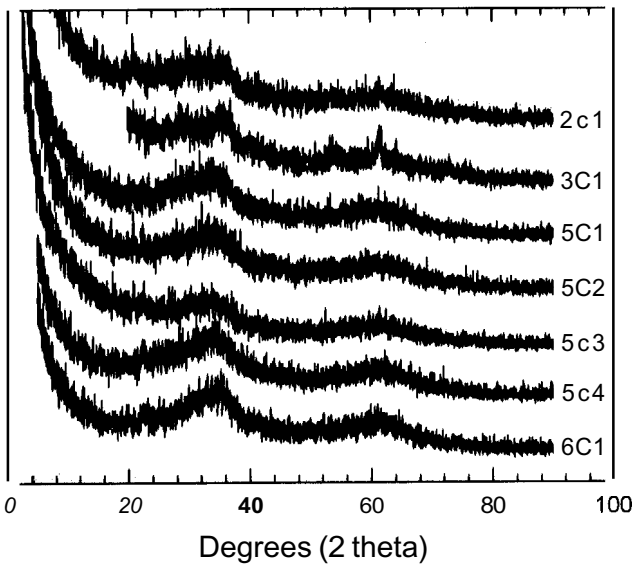

Figure 12. X-ray powder diffraction patterns for the seven "surface" samples. Note the broad maxima at ~36" and ~62°, corresponding to interplanar ("d") spacings of ~0.25 nm and ~0.15 nm, respectively.

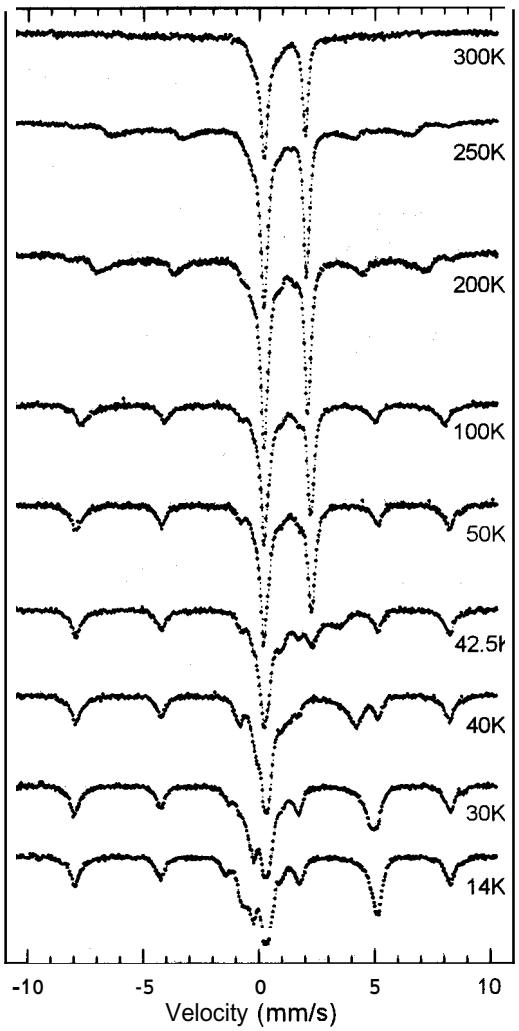

Figure 13. Mossbauer spectra of sample 2C3, taken at various temperatures.

face" samples, especially for 6C1 and 5C1-4, resemble very closely that reported for a "two-peak" ferrihydrite (maxima corresponding to interplanar spacings of ~0.25 nm and ~0.15 nm) [*Schwertmann*, 1988] and confirm the Mossbauer results. Note that additional, narrower peaks are observed in the diffraction patterns for 2C1 and 3C1 but not at positions expected for goethite.

3.4. Samples Exhibiting More Complex Spectra ("Subsurface" Samples)

3.4.1. The 2C3 sample. A widely spaced doublet, characteristic of ferrous iron dominates the 300 K spectrum of this sample (Figure 7, 2C3). However, the two peaks are not symmetric, the near zero-velocity peak being more intense with some broadening near its base, and there is evidence in the background of a weak, magnetic component. The phases present in sample 2C3 are more clearly indicated in the full temperature sequence, shown in Figure 13. **A** good fit to the 250 K spectrum is obtained with a five-site model (two ferric doublets, one ferrous doublet, and two broadened and skewed sextets), as shown in Figure 14; the results are given in Table 7. The two ferric doublets combine to give what resembles a broadened singlet, similar to that reported by ***Sherman and Vergo*** [1988] for the smectite clay mineral nontronite $[(Ca,Na)_{0.66}Fe_4Si_{7.34}Al_{0.66}O_{20}(OH)_4 \cdot nH_2O]$, who compute a range of values for the ratio of the two quadrupole splittings at 300 K of 2.3-2.7, consistent with the corresponding ratio of 2.63 for sample 2C3 at 300 **K** (Table 7). Parameter values for the ferrous doublet are consistent with those reported for siderite ($FeCO_3$) [*Ono and Ito,* 1964]. The parameters for the two magnetic components are consistent with nanophase goethite and nanophase hematite.

The most striking aspect of the spectral sequence (Figure 13), which is observed between 50 K and 30 **K,** is an apparent migration of the high-velocity siderite peak from ~2 to ~5 mm/s, to ultimately overlap the fifth peak of a magnetic sextet. At the same time, the central region of the spectrum becomes more complex. **A** temperature sequence (Figure 15) for ground natural siderite (Copper Lake, Antigonish County, Nova Scotia) shows a similar behavior, with a magnetic transition as temperature is lowered and subsequent increase in

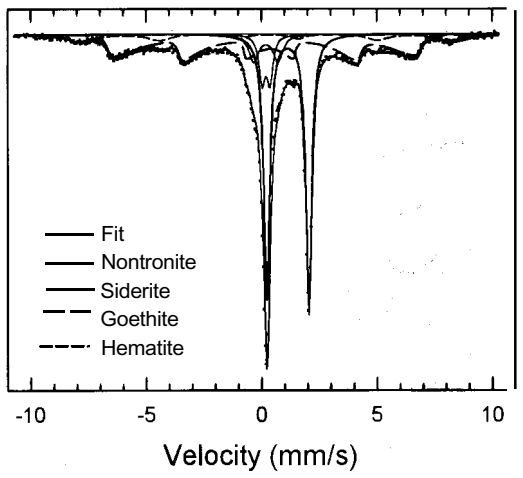

Figure 14. Least squares fit of the 250 K spectrum of sample 2C3. The full fit is shown as the dark line through the data. The component spectra are identified in the legend.

Table 7. Sample 2C3 Mossbauer Parameters

Temperature, K	IS, mm/s	QS, mm/s	B_{hf}, T	W, mm/s	Area, %
300	0.23	0.41	--	0.35	13.5
	0.23	1.08	--	0.54	13.6
	1.23	1.78	--	0.27	48.7
	0.32	-0.33	29.9	2.12	24.2
250	0.32	0.34	--	0.31	7.0
	0.32	1.05	--	0.52	6.8
	1.25	1.83	--	0.31	39.8
	0.36	-0.25	41.0	0.50	37.0
	0.41	-0.02	**50.5**	0.70	9.4
200	0.34	0.37	--	0.39	8.9
	0.34	1.16	--	0.47	4.6
	1.30	1.88	--	0.32	40.8
	0.39	-0.27	44.7	0.48	36.5
	0.41	-0.02	50.9	0.70	9.2
100	0.41	0.35	--	0.32	9.0
	0.41	1.03	--	0.80	8.8
	1.38	2.01	--	0.32	44.8
	0.46	-0.31	48.9	0.40	24.2
	0.43	-0.02	50.2	0.70	13.2
50	0.41	0.35	--	0.33	8.7
	0.41	1.03	--	0.80	8.4
	1.39	2.05	--	0.35	46.8
	0.46	-0.33	50.1	0.32	23.4
	0.43	-0.02	50.2	0.70	12.7
40	0.46	0.25	--	0.40	22.7
	0.46	1.19	--	0.31	4.2
	1.35	2.03	11.9	0.64	36.2
	0.49	-0.27	50.3	0.36	23.5
	0.46	-0.02	***50.5***	0.57	13.4
14	0.46	0.20	--	0.36	19.2
	0.46	0.94	--	0.50	9.8
	1.39	2.10	17.2	0.39	32.2
	0.49	-0.28	50.3	0.22	20.8
	0.47	-0.02	50.5	0.43	18.0
$FeCO_3$, 300 K	1.38	1.87 [a]	--	--	--
$FeCO_3$, 20 K	--	2.10 [b]	17.2 [c]	--	--
bGt, 22 K	0.47	-0.25	49.8	--	--
nHm, 22 K	0.48	-0.08	50.0	--	--

Fits modeled as discussed in the text **Also** included are reference values for siderite ($FeCO_3$) [*Ono & Ito*, 1964] and for **bulk** goethite (bGt) and np hematite (nHm) at 22 K [*Morris et al.*, 1989b]

[a] Reported error ±0.10

[b] Reported error ±0.20

[c] Reported error ±1.5

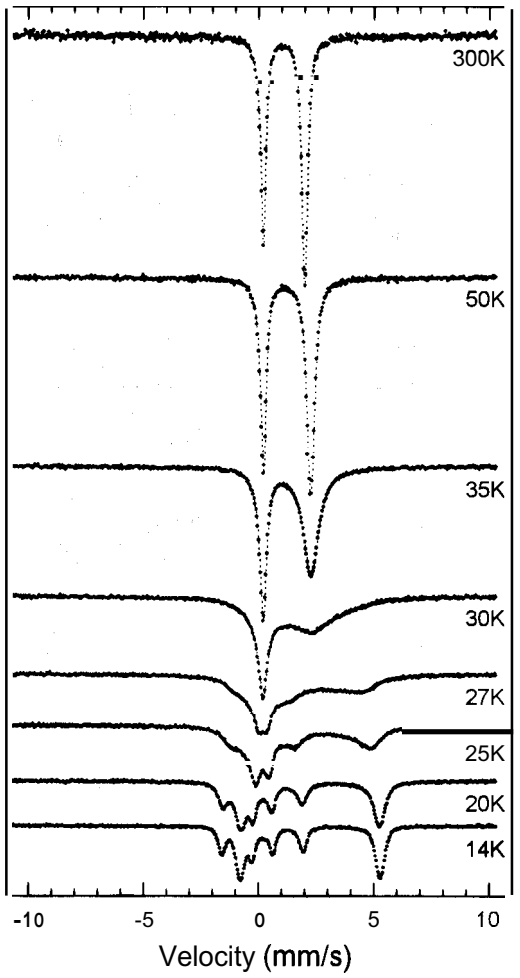

Figure 15. Mossbauer spectra of natural siderite (Nova Scotia), taken at various temperatures.

B_{hf}. A fit of the 14 K spectrum of this natural siderite is shown in Figure 16.

The analysis of the 14 K spectrum of sample 2C3 is shown in Figure 17, which illustrates the contributions of the pair of doublets corresponding to nontronite, the siderite sextet, a nanophase goethite sextet, and a broad nanophase hematite sextet. The fit results are given in Table 7, which lists components in this same order. Note that the inferred transition temperature for the nanophase goethite component (~300 K) is greater than that observed for Manitou Springs or Obsidian Pool (see Figure 6).

Figure 18 shows the variation of the magnetic hyperfine field B_{hf} with temperature for the Nova Scotia siderite and the siderite component of 2C3; also plotted are values for a synthetic siderite (99.58 pure $FeCO_3$) [*Ok*, 1969]. It appears that the three siderites converge very nearly to the same low temperature limit for B_{hf} but have distinctly different magnetic transition temperatures, presumably due to different modes of production and possibly different degrees of substitution for iron in the siderite structure of the natural samples. Like goethite and fenihydrite, natural siderite exhibits a range of magnetic transition temperatures.

The X-ray powder diffraction pattern of the 2C3 sample is shown in Figure 19, where the three iron-bearing phases, sid-

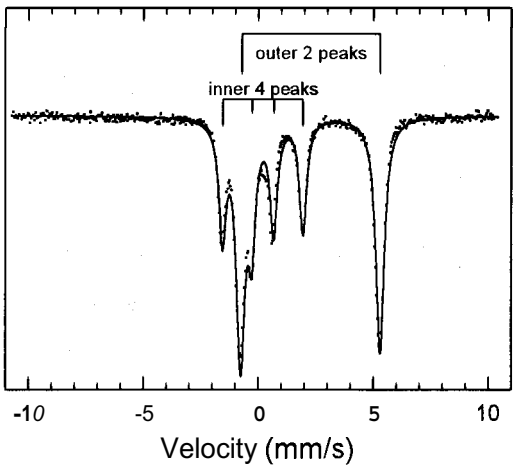

Figure 16. Least squares fit of the 14 K spectrum of natural siderite (Nova Scotia). Individual peaks are interpreted in the line diagrams at the top.

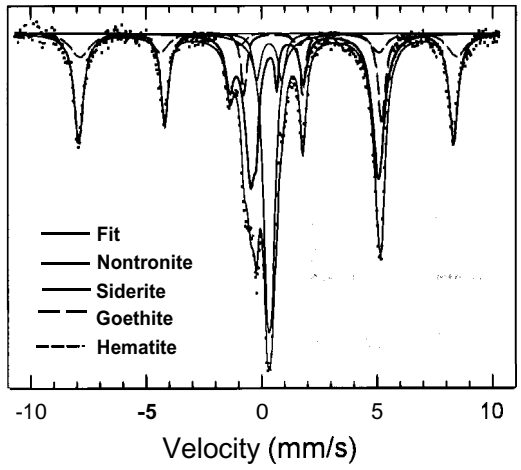

Figure 17. Least squares fit of the 14 K spectrum of sample 2C3. The full fit is shown as the dark line through the data. The component spectra are identified in the legend.

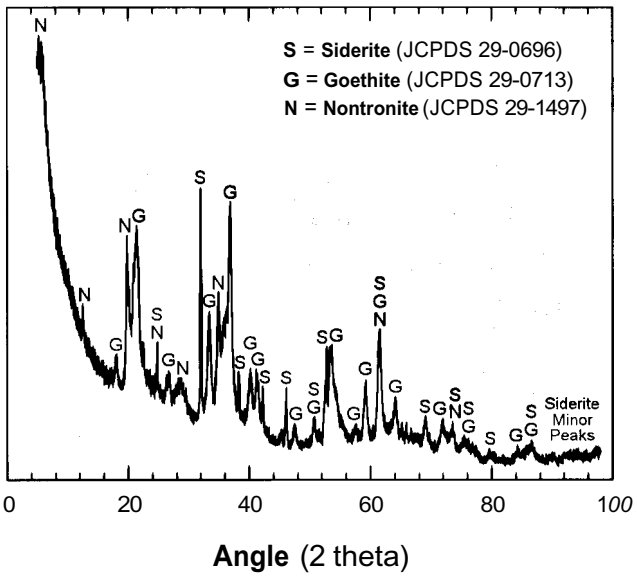

Figure 19. Powder XRD spectrum of sample 2C3. Assignments are siderite, S; goethite, G; and nontronite, N. *JCPDS* [1980] Card file numbers are at top right.

erite, goethite, and nontronite, are identified by the peak labels S, G, and N, respectively. Note that the tentative identification of the broadened Mossbauer singlet as nontronite is confirmed. The assignment of the XRD peaks appears to be complete; no other phases are identified. In other words, Mossbauer spectroscopy reveals all the mineral components present in 2C3 that are observable with the X-ray diffraction technique.

3.4.2. Other "subsurface" samples. Figures 20 and 21 are the temperature sequences for samples 2C2 and 2C4. Similar low-temperature spectra are obtained for 3C2-3C4. The spectral analysis is similar to that of 2C3. The results indicate that these five additional "subsurface" samples contain the same phases as 2C3, namely, siderite, nontronite, goethite, and hematite, in varying proportions. Full details of these analyses are published by ***Wade*** [1999].

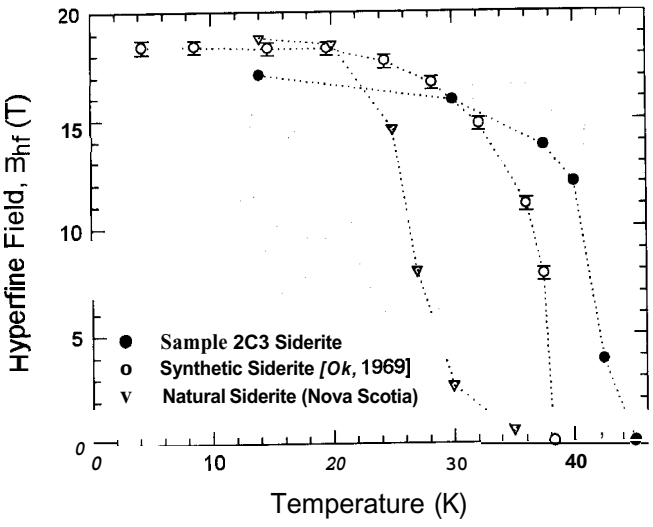

Figure 18. Values of the magnetic hyperfine field B_{hf} for three different forms of siderite: the 2C3 siderite component; synthetic $FeCO_3$ [*Ok*, 19691; and natural siderite (Nova Scotia).

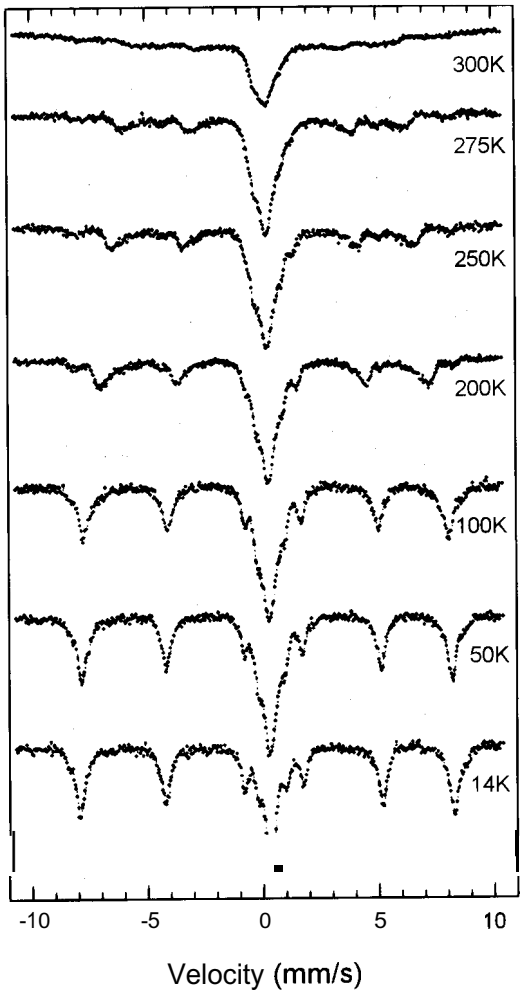

Figure 20. Mossbauer temperature sequence for sample 2C2.

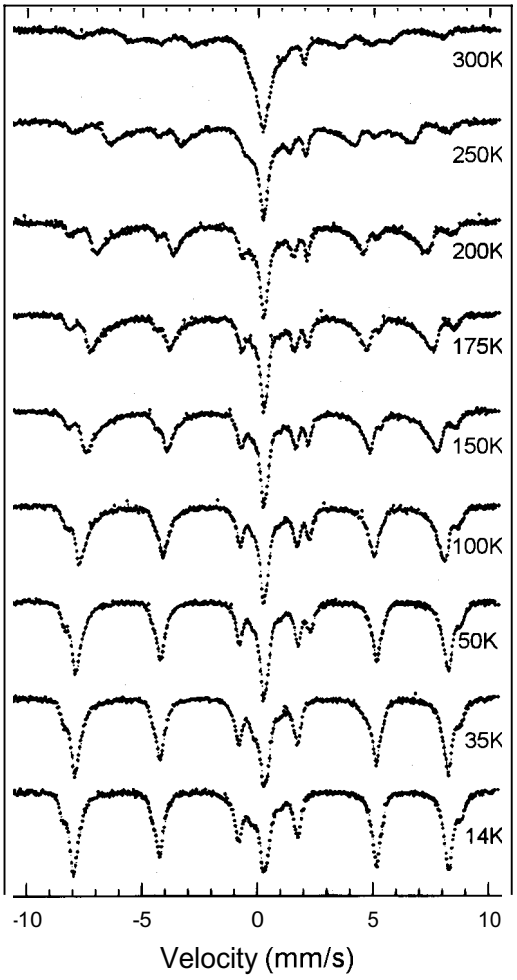

Figure 21. Mossbauer temperature sequence for sample 2C4.

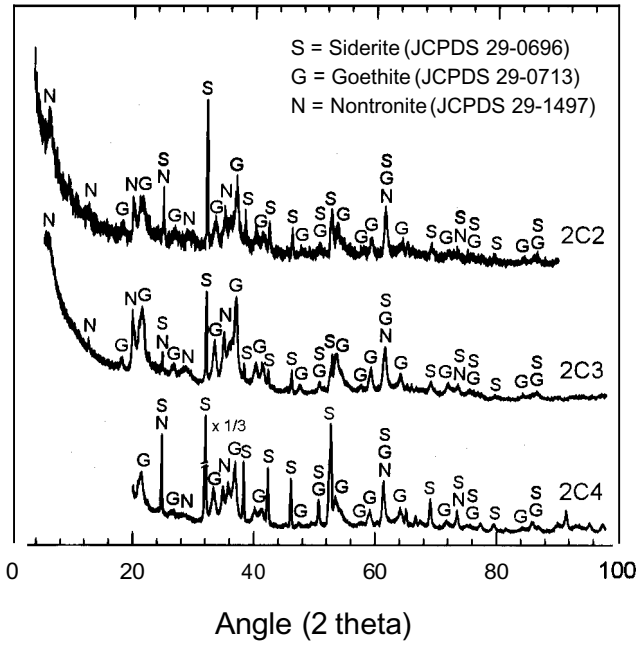

Figure 22. XRD powder spectra for samples 2C2-4. Assignments at top right.

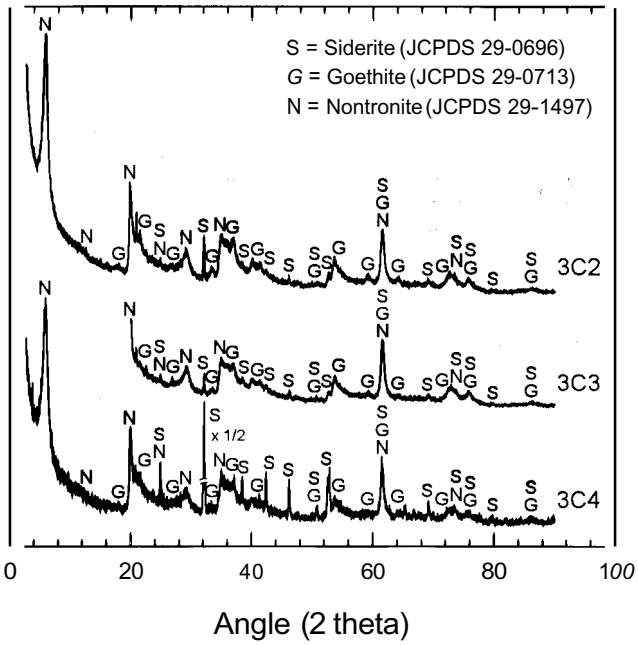

Figure 23. XRD powder spectra for samples 3C2-4. Assignments at top right.

An X-ray powder diffraction pattern was obtained for each of the "subsurface" samples (Figures 22 and 23). Siderite, goethite, and nontronite are identified by their well-defined peaks *[JCPDS,* 1980], confirming the assignments from Mossbauer spectroscopy. However, hematite is not seen, probably due to its low abundance in these samples (relatively small Mossbauer spectral area). The nanophase character of the goethite present is confirmed by the broadening of the corresponding lines in the XRD patterns, which also show broadened lines for evidently nanophase nontronite.

For a quantitative estimate of particle size, we use the Scherrer formula, given as equation (1). As the unbroadened, reference line, we use the 32.1" line of siderite in the 2C3 spectrum, whose FWHM, B_S, is 0.22". A well-defined goethite line appears at $2\theta_B$ = 59.2" with FWHM, B_G, of 0.70". Subtracting B_S from B_G in quadrature yields a line broadening of B = 0.66" = 0.0115 rad and an estimate for the mean particle size for goethite of $t_G \approx$ 14 nm. Similarly, the 29.2° peak of nontronite in the 3C3 diffractogram has $B_N \approx$ 1.66°, which yields $t_N \approx$ 5 nm. Since the degree of line broadening appears fairly consistent across all samples, we may take these two values as representative of the mean particle sizes of Chocolate Pots goethite and nontronite, respectively.

3.5. FESEM and EDX Results

Sample 2C1 (see Table 1) consists of porous, finely granular to microfibrous mineral aggregates, with elemental composition as determined by EDX analysis listed in Table 8.

Sample 3C1 consists mostly of finely granular to microfibrous mineral aggregates (analysis 3C1A, Table 8). However, the sample also includes abundant 0.5-0.7 μm wide, rod-shaped bacteria and fine (0.2 pm) and coarse filaments (0.7 pm) (Figure 24a), some showing preferred orientations (Figure 24b). Most samples also contain sheet-like to finely filamentous networks of dried mucilage with microgranular (0.1-0.3 pm) mineral grains and larger clumps (aggregates) up to

Table 8. EDX Compositional Analysis of Chocolate Pots Samples

Sample	C	O	Al	Si	P	S	Ca	Fe
2c1		m	w	s	w		w	m
3C1A	w	w	w	s	s	w	w	s
3C1B		w	w	s	w			
5C1A		s	w	s	w			s
5C1B		w		w				s
7C1	w	m	w	s	w		w	m

Elements identified in EDX spectra by the presence of their corresponding **X-ray** peaks. Relative intensities are indicated with w (~5-40), m (~40-70), or s (~70-100), where 100 is assigned to the strongest line in each pattern.

several microns across (Figure 24c). Sample 3C1 also contains laminae of a botryoidal, rosette-forming, glassy (concoidally fracturing) mineral (Figure 24d) with elemental composition suggestive of silica (3C1B, Table 8).

Sample 5C1 is finely laminated with interlayers of dark (glassy) and light (porous) sinter (Figures 25a and 25b). EDX spectra (5C1A, Table 8) of the porous surface layer (Figure 25c) and the porous interior layers (Figure 25b, top) are identical. In contrast, EDX analysis of the dark, interior layers (Figure 25b, bottom: 5C1B, Table 8) show much less silicon. Other glassy layers within the sample contain also B, C, and Ca, indicating that the composition of these laminae is quite variable.

For sample 7C1 the sinter framework consists of elongate aggregates of an iron oxide, probably ferrihydrite, which was deposited as coatings on bacterial filaments. Organic remains were subsequently decayed away, leaving behind filament molds, which were then progressively infilled (Figure 25d). EDX analysis of the filament coatings is presented in Table 8.

3.6. Discussion of FESEM and EDX Results

The near-surface samples examined by FESEM and EDX exhibit physical and chemical properties consistent with identification of the primary iron-oxide precipitate as femhydrite, inferred from Mössbauer spectroscopy and XRD. However, examination by light microscopy and FESEM of samples collected nearer the vent (5C1, Figures 25a and 25b) show that darker laminae of amorphous iron oxides and iron-rich silicates (clay minerals) are interbedded with lighter laminae of amorphous silica. XRD analysis of these samples confirms the amorphous nature of these materials, suggesting that the silica is amorphous (probably Opal-A) and that the iron-rich silicate is probably a smectite clay, possibly nontronite.

Siderite (iron carbonate) was identified at depths greater than 1 mm (in samples 2C2-4 and 3C2-4) using both Mössbauer and XRD but not observed in the surface samples. EDX results for samples 2C1 and 3C1A (Table 8) include calcium and are thus consistent with the presence of carbonate. However, visual evidence from FESEM is lacking for all samples of Table 1, any carbonate crystallites being evidently

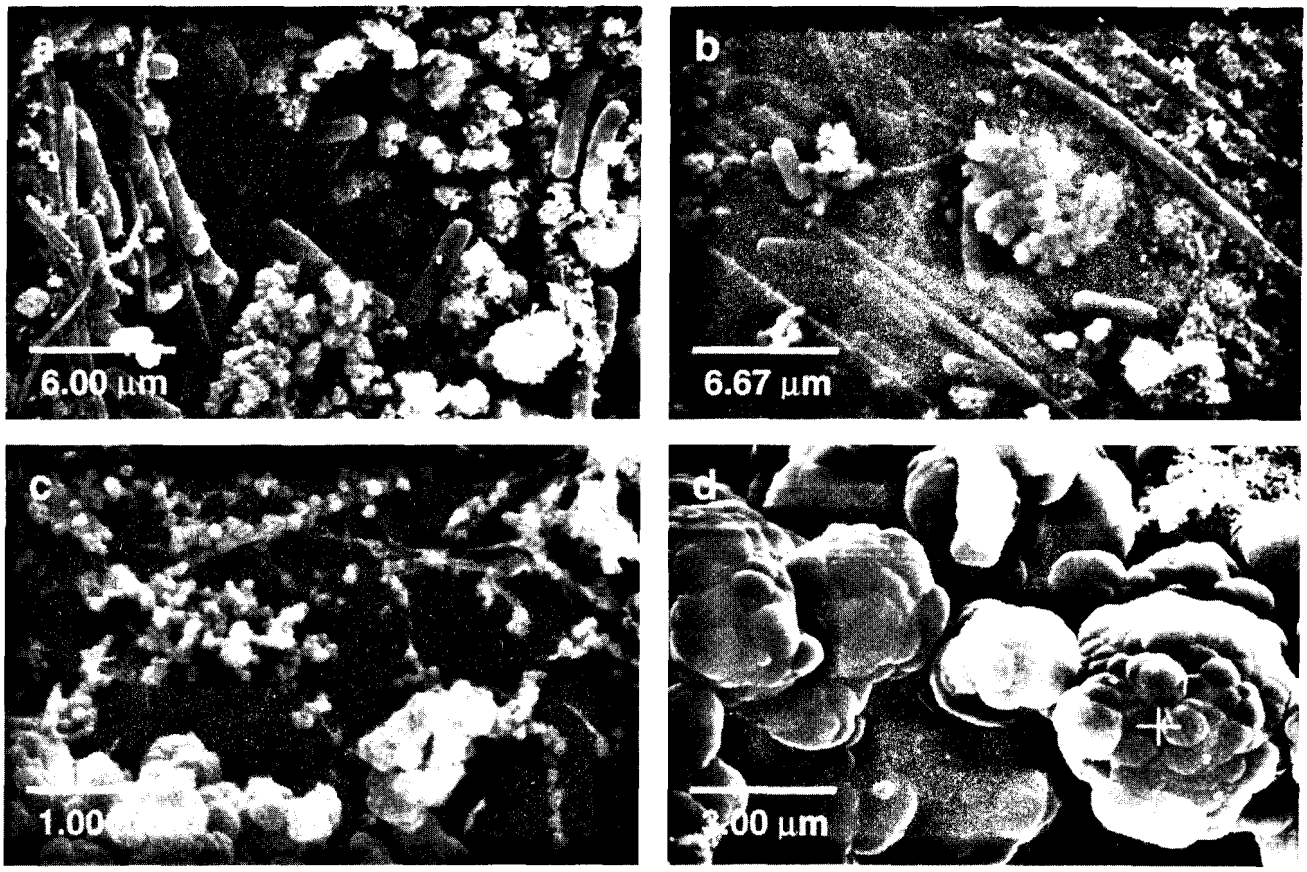

Figure 24. FESEM images of sample 3C1, showing (a) finely porous, microfibrous to microgranular aggregates encrusting mucilage/cells; (b) bacterial filaments similar to those shown in Figure 25a, but with preferred orientations: (c) webs and strings of dried mucilage with attached mineral grains and aggregates; and (d) rosettes of a glassy mineral, probably silica.

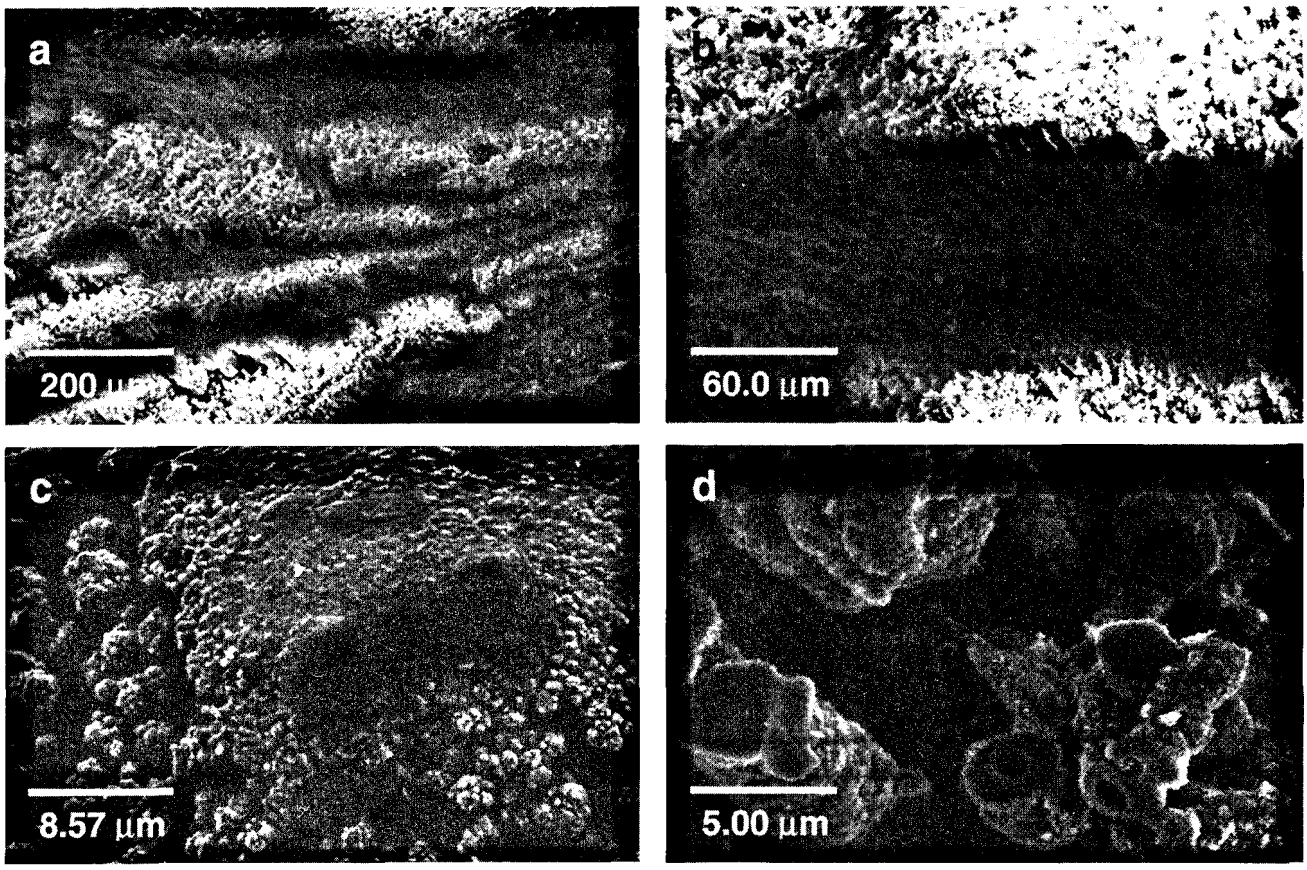

Figure 25. FESEM images, showing (a) the alternating interior layers of dark (glassy) and light (porous) sinter of sample 5C1; (b) a magnified view from Figure 26a; (c) the porous surface layer of sample 5C1 showing small botryoids of a silica-rich mineral; and (d) cross-sectional views of several encrusted bacterial filaments preserved as molds; note the partial to complete infilling.

so fine-grained they are indistinguishable from other microgranular materials present.

4. Siderite as a Component of an Ancient Stromatolite

Mossbauer spectra at two temperatures of a freshly slabbed portion of a 2.09 Ga (Early Proterozoic) hematic chert stromatolite from the Gunflint Iron Formation (PPRG 2443) are shown in Figure 26. The high-velocity ferrous peak migrates from its position at 100 K to overlap the fifth peak of hematite at 19 K. This behavior and the agreement of the splitting parameters with those of siderite argue that this sample contains a small fraction of siderite.

Wdowiak et al. [1997] have reported a Raman spectrum of this sample (Figure 27), obtained with 3 mW of HeNe 633-nm laser power. It reveals the SiO_2 signature of the chert at $-460\ cm^{-1}$ and the carbon G ($1600\ cm^{-1}$) and D ($1332\ cm^{-1}$) bands, the latter blended with a broad hematite band at ~1320-1340 cm^{-1} *[Williams et al.,* 19971. The biotic origin of this carbon is suggested by the occurrence of well-preserved organic-walled microfossils in petrographic thin sections of Gunflint chert *[Barghoorn and Tyler,* 1965; *Barghoorn et al.,* 19771. Similar Raman signatures (sans hematite) of carbonaceous chert were observed in –3.3-–3.5 Ga Archean black cherts of the Barberton Greenstone Belt, South Africa *[Wdowiaketal.,* 1997].

As in the spectra of the contemporary thermal springs (Figure 14), the Mossbauer signature of siderite is apparent in PPRG sample 2443, although not seen in the Raman spectrum (dominant siderite peak at $-1090\ cm^{-1}$). The sample investigated was freshly slabbed for the Mossbauer transmission measurement, so the iron carbonate is interior to the native stromatolite rock. Its occurrence in this 2.09 Ga old rock indicates that long (billion-year) survival times for siderite are possible when preserved in silica.

5. Implications for Mars Exploration

Mossbauer spectra of minerals are often taken at just one temperature (e.g., room temperature), and their characteristic spectrum ("fingerprint") at that temperature is then used for identification. The same "fingerprinting" procedure will find utility for spectra obtained on Mars, except that the measurement temperature would not be our "room temperature." For the samples investigated here, all the component minerals were first identified from the Mossbauer spectra and later corroborated by XRD (if seen at all by XRD). Although we have operated in the transmission mode, as is typical in the laboratory setting, the spectra obtained could have been obtained in backscatter mode, which is employed by the Athena Mössbauer spectrometer (S.W. Squyres, http://astrosun.tn.comelL edu/athena/mossbauer.html, 1998a). Again, we point out the inherent simplicity of backscatter operation as compared to

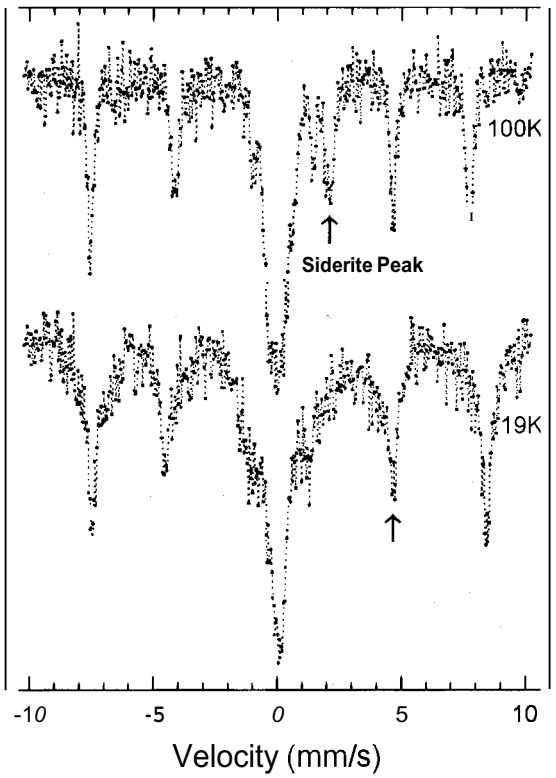

Figure 26. Mossbauer spectra of a hematite-rich chert stromatolite (Gunflint Iron Formation) at two temperatures, showing migration of the siderite high-velocity peak (↑).

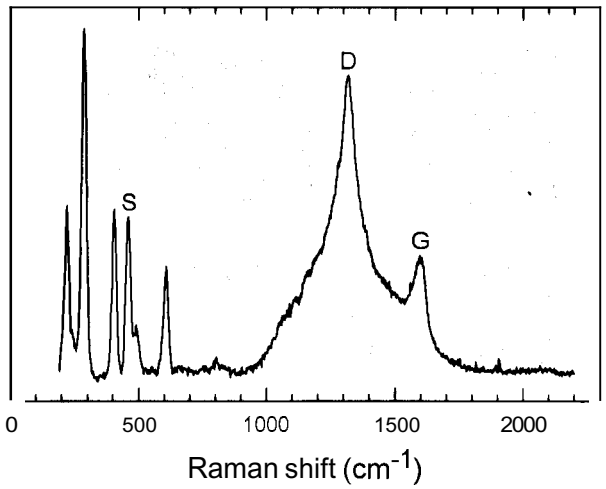

Figure 27. Raman spectrum (baseline subtracted) of a hematite-rich chert stromatolite (Gunflint Iron Formation) [*Wdowiak et al.,* 19971, showing the SiO_2 peak (S) at −460 cm^{-1} with the D (disordered) and G (graphitic) bands of carbon (signature for carbonaceous chert) and the spectrum of hematite, which includes a broad band coincident with the carbon D band.

the likely situation involving sample preparation prior to performing XRD measurements for mineralogy.

As we have seen in this report, measurement of Mossbauer spectra over a range of temperatures is important for more fully exploiting the technique. Some spectral components of the hydrothermal materials investigated here show little change **as** function of temperature (e.g., nontronite, hematite), while others change significantly only at low temperature, where a magnetic transition takes place (femhydrite, siderite). However, the nanophase component (i.e., goethite) shows significant and distinctive variation over the entire temperature range, its room temperature doublet gradually converting to sextet area as temperature is lowered, while its sextet component gradually narrows in peak width and increases in peak separation [*Mørup*, 1983].

On Mars, it is unlikely, because of requirements for simplicity/economy of the instrument, that there will be the possibility of setting and controlling the sample temperature during a Mossbauer measurement, as is done in the terrestrial laboratory. However, the Martian ambient temperature [e.g., *Schofield et al.,* 19971 exhibits wide diurnal variation with rapid swings between maximum and minimum temperatures (Figure 28). **As** a result (assuming the examined sample follows a similar temperature trend), there would be sufficient time available to obtain high-quality Mossbauer spectra at the two extremes. For the particular day shown, the analysis included in Figure 28 shows that spectra could be taken at 260 K (±5 K) for −5 hours and at 200 K (±5 K) for −8 hours.

For some of the mineral constituents of our samples (nontronite, hematite, ferrihydrite), minimal spectral variation would mean little advantage in obtaining spectra at these two temperatures instead of just one. However, the case of nanophase goethite is quite different, as we see by inspection of the 250 K and 200 K spectra of the Manitou Springs (Figure 2) and Obsidian Pool (Figure *5)* sequences. This is quantified in the magnetic hyperfine field (B_{hf}) plot for these two samples (Figure 6), which also includes bulk goethite. For **all** three cases, the differences between B_{hf} at 200 K and B_{hf} at 260 K are significant. Indeed, the ratio, $B_{hf}(200)/B_{hf}(260)$, could be used to sequence the three samples with respect to apparent ordering temperature T_p and possibly yield quantitative estimates for this parameter as well.

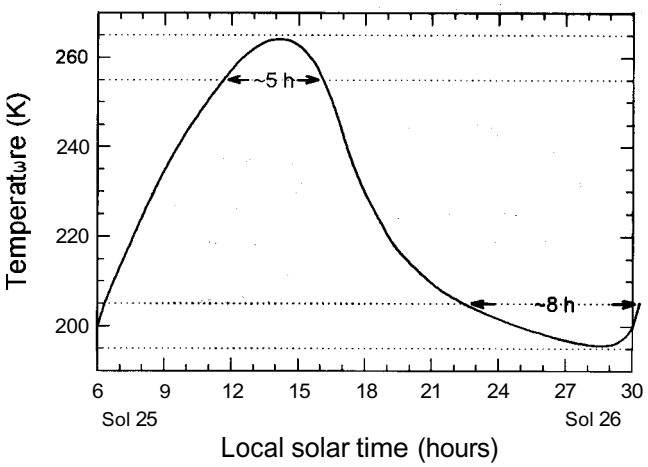

Figure 28. Diurnal temperature variation (solid line) at the Mars Pathfinder site, adapted from the atmospheric temperature measurements of *Schofield et al.* [1997]. The dotted lines show that sufficient time is available to acquire good quality Mossbauer measurements at −260 K and −200 K.

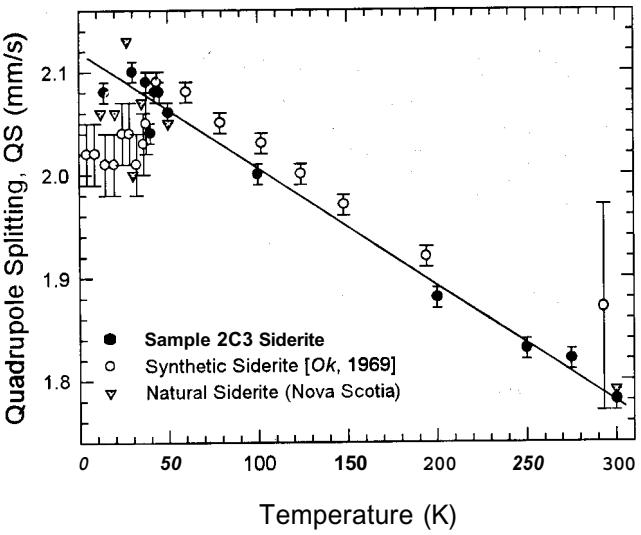

Figure 29. Values of the quadrupole splitting parameter QS for three different forms of siderite: the 2C3 siderite component; synthetic $FeCO_3$ [*Ok*, 1969]; and natural siderite (Nova Scotia). The solid line results from a fit to the 2C3 data for QS above the magnetic transition temperature (from 45 **K** to 300 K).

For siderite the advantage of acquiring spectra at the two Martian temperatures is more subtle. However, as shown in Figure 29, the quadrupole splitting is quite temperature sensitive. While it is true that measurement of isomer shift (IS) and quadrupole splitting (QS) may be sufficient to fingerprint an observed spectral component as due to siderite, measurement of the ratio, QS(200)/QS(260), would be corroborative evidence for the occurrence of this very important mineral.

Finally, for a deposit to be identified by a modem-day Mossbauer spectrometer on Mars as resulting from an early hydrothermal system, its constituent minerals must survive for billions of years. This is generally true of the mineral components present in the hydrothermal deposits discussed in this report. In particular, the fact that nanophase material can be preserved for eons was demonstrated by the discovery of a nanophase component in the 4.5-billion-year-old Orgueil meteorite [*Wdowiak and Agresti,* 1984; *Madsen et al.,* 1986], later identified as ferrihydrite [*Tomeoka and Buseck,* 19881. This suggests that fenihydrite, and thus its Mossbauer signature, may remain over geologic time as a marker for amorphous material produced in an ancient Martian hydrothermal setting. The discovery of siderite in a 2.09 Ga hematitic chert stromatolite, reported here, suggests similar longevity for siderite, at least in siliceous sediments (cherts).

6. Conclusion

Our ability to detect iron carbonate (siderite) in Mossbauer spectra of our iron spring samples from Chocolate Pots in Yellowstone underlines the potential importance of Mössbauer for the in situ analysis of Martian crustal rocks during future landed missions. A systematic search for iron carbonates in Martian rocks using Mossbauer spectroscopy would afford an opportunity to test hypotheses regarding the evolution of the Martian atmosphere and climate.

Isotopic data from SNC meteorites suggest the need for an ongoing mechanism of crustal-atmosphere exchange, which *Jakosky and Jones* [1994] have attributed to active subsurface hydrothermal systems. It is generally assumed that CO_2 of the primitive Martian atmosphere was lost through a combination of escape to space and sequestering in the crust as carbonates. Geochemical models [*Griffith and Shock,* 1995; *Griffith et al.,* 1995] indicate that hydrothermal mineralization could have been a highly effective means for sequestering carbonates in the early Martian crust. The presence of carbonates in Martian meteorite ALH 84001 [*McKay et al.,* 1996] hints at the possibility that disseminated carbonates may be present in the older crustal regions of Mars. The bulk composition of the Martian crust is thought to be primarily basaltic, and therefore enriched in Fe, Mg, and Ca. It is likely that solutes formed through hydrothermal circulation in the Martian crust would be comparatively enriched in these elements and that any carbonates precipitated from those solutions would tend to be iron-rich varieties *[Farmer,* 1996]. While the temperature of formation of the carbonates in ALH 84001 is still uncertain, implicit in the ongoing debate over the biogenicity of features is the assumption of a hydrothermal origin.

The occurrence of siderite within our subsurface profiles at Chocolate Pots suggests a potentially important connection to the microbiology of the system. Carbonate precipitation has been shown to be biologically-mediated due to pH increases induced by sulfate reduction *[Krumbein,* 1979; *Erlich,* 19961. It is possible that a similar mechanism may account for the precipitation of iron carbonates within the deeper portions **of** our mat profiles. There is, in fact, a general increase in *p*H with depth in the Chocolate Pots sinters (B. Pierson, University of Puget Sound, personal communication, 1997). If the carbonates are being precipitated through biological controls, the isotopic signatures of the carbonates should reflect enrichment in the heavier isotope. It is also quite possible that these authigenic carbonates have captured microfossils or organic compounds as they precipitated. These comprise important areas for research, which we will address in the future. In the siderite-bearing samples, nontronite (an iron-rich smectite clay) and crystalline iron oxides (hematite and goethite) are also present. This suggests the primary amorphous phase (ferrihydrite), deposited at the surface in this system, is diagenetically transformed to ordered phases as the mound accretes and the surface sediments are progressively buried.

Traditionally, X-ray powder diffraction has been considered the most definitive method for determining mineralogy. However, the likely requirement for preparation of a sample could complicate its use on Mars. The most efficient approaches for mineralogical identification are surface reflectance techniques that require only the exposure of a fresh rock surface. Backscatter X-ray methods have not been shown to provide definitive mineralogy, but studies of Mossbauer spectroscopy in backscatter mode indicate the technique to be quite reliable for determinative mineralogy of iron-bearing minerals [*Klingelhöfer*, 1998, and references therein], which are, of course, abundant on Mars.

We have shown that Mossbauer spectroscopy is capable of identifying a variety of materials associated with iron-rich hydrothermal springs on Earth. There is evidence that these materials, and hence their spectral signatures, can be preserved for billions of years. It is plausible that similar materials were produced in early hydrothermal systems on Mars. If this material survived to the present day and was investigated by an in situ Mossbauer spectrometer emplaced on the Mar-

tian surface, there is high likelihood the instrument would yield evidence for the earlier hydrothermal system. It would thus have discovered a sample with compelling reason to be collected and returned to Earth for further investigation, including a search for fossils possibly contained therein.

The major reason for assembling integrated instrument suites is demonstrated by our combined use of Mossbauer and Raman spectroscopy to characterize the stromatolite sample. An integrated instrument suite for in situ science is like an orchestra composed of rather different kinds of musical instruments, such that the performance that results exceeds greatly what individual instruments can achieve alone [*Wdowiak,* 1996].

Acknowledgments. This research has been funded by NASA Exobiology/PIDDP grant NAGW-4854/NAG5-4584 (to T.J.W.) and NASA Exobiology Program grant 344-38-32-08 (to J.D.F.). We wish to thank Richard V. Morris (Johnson Space Center) for helpful discussions.

References

Agresti, D., in Travis, J., Ironing out life on Mars, *Science,* 268, 31, 1995.

Agresti, D.G., and T.J. Wdowiak, Iron Mossbauer spectroscopy: Superparamagnetism in hydrothermal vents and the search for evidence of past life on Mars, in *Mars Surface and Atmosphere Through Time,* pp. 9-10, *Tech. Rep. 92-02,* Lunar and Planet. Inst., Houston, **Tex.,** 1992.

Agresti, D., M. Bent, and B. Persson, A versatile computer program for analysis of Mossbauer spectra, *Nucl. Instrum. Meth.,* 72, 235-236,1969.

Agresti, D.G., T.J. Wdowiak, and M.L. Wade, Mossbauer spectroscopy as a tool in the search for evidence of past life on Mars, *Hyperfine Interact., 91,* 523-528, 1994.

Agresti, D.G., T.J. Wdowiak, M.L. Wade, L.P. Armendarez, and J.D. Farmer, A Mossbauer investigation of hot springs iron deposits, *Lunar Planet. Sci., XXVI,* 7-8, 1995.

Agresti, D.G., T.J. Wdowiak, M.L. Wade, L.P. Armendarez, and J.D. Farmer, Mossbauer spectroscopy of thermal springs iron deposits as Martian analogs, in *Conference on Early Mars: Geologic and Hydrologic Evolution, Physical and Chemical Environments, and the Implications for Life,* edited by S.M. Clifford et al., *LPI Contrib., 916,* 1-2, 1997.

Allen, E.T., and A.L. Day, *Hot Springs of the Yellowstone National Park,* 525 pp., Carnegie Institution of Washington, Washington, D.C., 1935.

Alt, J.C., Hydrothermal oxide and nontronite deposits on seamounts in the eastern Pacific, *Mar. Geol., 81,* 227-239, 1988.

Bancroft, G.M., *Mössbauer Spectroscopy: An Introduction for Inorganic Chemists and Geochemists,* 251 pp., McGraw-Hill, New York, 1973.

Banin, A., X.F. Han, I. Kan, and A. Cicelsky, Acidic volatiles and the Mars soil, *J. Geophys. Res.,* 102, 13,341-13,356, 1997.

Barghoorn, E.S., and S.A. Tyler, Microorganisms from the Gunflint chert, *Science,* 148,461-472, 1965.

Barghoorn, E.S., A.H. Knoll. H. Dembicki Jr., and W.G. Meinschein, Variation in stable carbon isotopes in organic matter from the Gunflint Iron Formation, *Geochim. Cosmochim. Acta, 41,* 425-430, 1977.

Barns, **S.M.,** C.F. Delwiche, J.D. Palmer, S.C. Dawson, K.L. Hershberger, and N.R. Pace, Phylogenetic perspectives on microbial life in hydrothermal ecosystems, past and present, in *Evolution of Hydrothermal Ecosystems on Earth (and Mars?),* edited by G.A. Bock and J.A. Goode, pp. 24-39, John Wiley, New York, 1996.

Baross, J.A., and S.E. Hoffman, Submarine hydrothermal vents and associated gradient environments as sites for the origin and evolution of life, *Origin Life Evol. Biosphere, 15,* 327-345, 1985.

Bent, M.F., B.I. Persson, and D.G. Agresti, Versatile program for analysis of Mossbauer spectra, *Comput. Phys. Commun., 1,* 67-87, 1969.

Brakenridge, G. R., H.E. Newsom, and V.R. Baker, Ancient hot springs on Mars: Origin and paleoenvironmental significance of small Martian valleys, *Geology.* 13,859-862, 1985.

Carr, M., *Water on Mars,* 240 pp., Oxford Univ. Press, New York, 1996.

Coey, J.M.D., Magnetic properties of iron in soil iron oxides and clay minerals, in *Iron in Soils and Clay Minerals,* edited by J.W. Stucki, B.A. Goodman, and U. Schwertmann, pp. 397-466, D. Reidel, Norwell, Mass., 1988.

Corliss, J.B., Hot springs and the origin of life, *Nature,* 347, 624, 1990.

Corliss, J.B., J.A. Baross, and S.E. Hoffman, An hypothesis concerning the relationship between submarine hot springs and the origin of life on Earth, *Oceanol. Acta, 4,* 59-69, 1981.

Cullity, B.D., *Elements of X-Ray Diffraction,* 2nd ed., 555 pp., Addison-Wesley, Reading, Mass., 1978.

Erlich, H.L, *Geomicrobiology,* 3rd ed., 646 pp., Marcel Dekker, New York, 1996.

Erwin, J.B., *Report of the Acting Superintendent of the Yellowstone National Park to the Secretary of the Interior,* Government Printing Office, Washington, D.C., 1898.

Evlanov, E.N., L.M. Mukhin, O.F. Prilutski, G.V. Smirnov, J. Juchniewicz, E. Kankeleit, G. Klingelhofer, J.M. Knudsen, and C. d'Uston, Mossbauer backscatter spectrometer for mineralogical analysis of the Mars surface for Mars-94 mission, *Lunar Planet. Sci., XXII,* 361-362, 1991.

Farmer, J.D., Mars exopaleontology, *Palaios, 10,* 197-198, 1995.

Farmer, J.D., Hydrothermal processes on Mars: An assessment of present evidence, in *Evolution of Hydrothermal Ecosystems on Earth (and Mars?),* edited by G.A. Bock and J.A. Goode, pp. 273-299, John Wiley, New York, 1996.

Farmer, J.D., and D.J. Des Marais, Exopaleontology and the search for a fossil record on Mars, *Lunar Planet. Sci., XXV,* 367-368, 1994.

Geissler, P.E., R.B. Singer, G. Komatsu, **S.** Murchie, and J. Mustard, An unusual spectral unit in west Candor Chasma: Evidence for aqueous or hydrothermal alteration in the Martian canyons, *Icarus, 106,* 380-391, 1993.

Griffith, L.L., and E.L. Shock, A geochemical model for the formation of hydrothermal carbonates on Mars, *Nature,* 377, 406-408, 1995.

Griffith, L.L., E.L. Shock, and R.E. Arvidson, Calculating the effects of hydrothermal alteration on Mars, *Lunar Planet. Sci., XXVI,* 517-518, 1995.

Jakosky, B.M., and J.H. Jones, Evolution of water on Mars, *Nature, 370,* 328-329, 1994.

Joint Committee on Powder Diffraction Standards (JCPDS), *Mineral Powder Diffraction File Data Book,* 1168 pp., Swarthmore, Pa., 1980.

Klingelhofer, G., In-situ analysis of planetary surfaces by Mossbauer spectroscopy, *Hyperfine Interact., 113,* 369-374, 1998.

Klingelhofer, G., et al., Mossbauer spectrometer for mineralogical analysis of the Mars surface for the Mars-96 mission, *Lunar Planet. Sci., XXIII,* 695-696, 1992.

Klingelhofer, G., P. Held, J. Foh, F. Schlichting, R. Teucher, E. Kankeleit, E.N. Evlanov, O.F. Prilutski, G.V. Veselova, and E.A. Duzheva, Optimization of the miniaturized backscattering Mössbauer spectrometer MIMOS, *Lunar Planet. Sci., XXV,* 709-710, 1994.

Knudsen, J.M., Mossbauer spectroscopy of ^{57}Fe and the evolution of the solar system, *Hyperfine Interact., 47,* 3-31, 1989.

Knudsen, J.M., S. Mørup, and J. Galazka-Friedman, Mossbauer spectroscopy and the iron on Mars, *Hyperfine Interact., 57,* 2231, 1990.

Knudsen, J.M., et al., Mossbauer spectroscopy on the surface of Mars. Why?, *Hyperfine Interact.. 68,* 83-94, 1991.

Koch, C.J.W., M.B. Madscn, and S. Mørup, Evidence for microcrystallinity in large particles of goethite, *Surf. Sci., 156,* 249-255, 1985.

Krumbein, W.E., Calcification by bacteria and algae, in *Biogeochemical Cycling of Mineral-Forming Elements,* edited by P.A. Trudinger and D.J. Swaine, pp. 47-68, Elsevier, New York, 1979.

Kündig, W., H. Bommel, G. Constabaris, and R.H. Lindquist, Some properties of supported small a-Fe203 particles determined with the Mossbauer effect, *Phys. Rev.,* 142, 327-333, 1966.

Madsen, M.B., S. Mørup, T.V.V. Costa, J.M. Knudsen, and M. Olsen, Superparamagnetic component in the Orgueil meteorite and Mossbauer spectroscopy studies in applied magnetic fields, *Nature,* 321,501-503, 1986.

McCammon, C., Mossbauer spectroscopy of minerals, in *Mineral Physics and Crystallography: A Handbook of Physical Constants, AGU Ref. Shelf,* vol. 2, edited by T.J. Ahrens, pp. 332-347, AGU, Washington, D.C., 1995.

McKay, D.S., E.K.J. Gibson, K.L. Thomas-Keprta, H. Vali, C.S. Romanek, S.J. Clemett, X.D.F. Chillier, C.R. Maechling, and R.N. Zare, Search for past life on Mars: Possible relic biogenic activity in Martian meteorite ALH84001, *Science,* 273, 924-930, 1996.

Mitra, **S.,** *Applied Miissbauer Spectroscopy: Theory and Practice for Geochemists and Archeologists,* 381 pp., Pergamon, Tarrytown, N.Y., 1992.

Morris, R.V., and D.C. Golden, Goldenrod pigments and the occurrence of hematite and possibly goethite in the Olympus-Amazonis region of Mars, *Icarus,* 134,1-10, 1998.

Morris, R.V., D.G. Agresti, T.D. Shelfer, and T.J. Wdowiak, Mossbauer spectroscopy for mineralogical analysis on planetary **sur**faces, in *Proceedings, Pathfinder Sample Acquisition, Analysis, and Preservation Instrument Technology Workshop,* NASA, Houston, Tex., Nov. 14-16, 1988.

Morris, R.V., D.G. Agresti, T.D. Shelfer, and T.J. Wdowiak, Mössbauer backscatter spectrometer: a new approach for mineralogical analysis on planetary surfaces, *Lunar Planet. Sci., XX,* 721-722, 1989a.

Morris, R.V., D.G. Agresti, H.V. Lauer Jr., J.A. Newcomb, T.D. Shelfer, and A.V. Murali, Evidence for pigmentary hematite on Mars based on optical, magnetic, and Mossbauer studies of superparamagnetic (nanocrystalline) hematite, *J. Geophys. Res., 94,* 2760-2778, 1989b.

Morris, R.V., D.C. Golden, and J.F. Bell III, Low-temperature reflectivity spectra of red hematite and the color of Mars, *J. Geophys. Res.,* 102,9125-9133, 1997.

Mørup, **S.,** Magnetic hyperfine splitting in Mossbauer spectra of microcrystals, *J. Magnet. Magnet. Mater.,* 37, 39-50, 1983.

Mørup, **S.,** and H. Topsoe, Mössbauer studies of thermal excitations in magnetically ordered microcrystals, *Appl. Phys., 11, 63-66,* 1976.

Mouginis-Mark, P.J., L. Wilson, and M.T. Zuber, The physical volcanology of Mars, in *Mars,* edited by H.H. Kieffer et al., pp. 424-452, Univ. of Ariz. Press, Tucson, 1992.

Murad, E., Properties and behavior of iron oxides **as** determined by Mossbauer spectroscopy, in *Iron in Soils and Clay Minerals,* edited by J.W. Stucki, B.A. Goodman, and U. Schwertmann, pp. 309-350, D. Reidel, Norwell, Mass., 1988.

Murad, E., and L.H. Bowen, The character of magnetic ordering in high-Al goethite and ferrihydrite, paper presented at the 8th International Clay Conference, Clay Miner. Soc., Denver, Colo., July 28-Aug. 2, 1985.

Mustard, J.F., and J.E. Hays, Effects of hyperfine particles on reflectance spectra from 0.3 to 25 μm, *Icarus,* 125,145-163, 1997.

National Aeronautics and Space Administration (NASA), *An exobiological strategy for Mars exploration, NASA Spec. Pub.,* 530, *56* pp., Washington, D.C., 1995.

Newsom, H.E., Hydrothermal alteration of impact melt sheets with implications for Mars, *Icarus, 44,* 207-216, 1980.

Newsom, H.E., Chemical transport in hydrothermal systems: Clues to the composition of the Martian soil, *Eos Trans. AGU, 78*(46), Fall Meet. Suppl., F403, 1997.

Ok, H.N., Relaxation effects in antiferromagnetic ferrous carbonate, *Phys. Rev.,* 185,472-476, 1969.

Ono, K., and A. Ito, Mossbaucr study of magnetic properties in ferrous compounds, *J. Phys. Soc. Jpn., 19,* 899-907, 1964.

Pirajno, F., *Hydrothermal Mineral Deposits. Principles and Fundamental Concepts for the Exploration Geologist,* 709 pp., Springer-Verlag, New York, 1992.

Russell, M.J., A.J. Hall, A.G. Cairns-Smith, and P.S. Braterman, Submarine hot springs and the origin of life, *Nature,* 336, 117, 1988.

Schofield, J.T., J.R. Barnes, D. Crisp, R.M. Haberle, **S.** Larsen, J.A. Magalhães, J.R. Murphy, A. Seiff, and G. Wilson, The Mars Pathfinder Atmospheric Structure Investigation/Meteorology (ASI/MET) Experiment, *Science,* 278, 1752-1758, 1997.

Schwertmann, U., Occurrence and formation of iron oxides in various pedoenvironments, in *Iron in Soils and Clay Minerals,* edited by J.W. Stucki, B.A. Goodman, and U. Schwertmann, pp. 267-308, D. Reidel, Norwell, Mass., 1988.

Shelfer, T.D., Combined backscatter Mossbauer spectrometer/x-ray fluorescence analyzer (BaMS/XRF) for planetary surface materials, Ph.D. thesis, Univ. of Alabama at Birmingham, 1992.

Sherman, D.M., and N. Vergo, Optical (diffuse reflectance) and Miissbauer spectroscopic study of nontronite and related Fe-bearing smectites, *Am. Mineral.,* **73,** 1346-1354, 1988.

Shock, E.L., and M.D. Schulte, Organic synthesis during fluid mixing in hydrothermal systems, *J. Geophys. Res.,* 103, 28,513-28,527, 1998.

Sleep, N.H., and K. Zahnle, Refugia from asteroid impacts on early Mars and the early Earth, *J. Geophys. Res., 103,* 28,529-28,544, 1998.

Squyres, S.W., et **al.,** The Athena Mars rover science payload, in *Lunar and Planetary Science XXIX,* [CD-ROM], Abstract 1101, Lunar and Planet. Inst., Houston, Tex., 1998.

Tomeoka, K., and P.R. Buseck, Matrix mineralogy of the Orgueil CI carbonaceous chondrite, *Geochim. Cosmochim. Acta,* 52, 1627-1640, 1988.

Wade, M.L., A Mossbauer spectroscopic study of iron-rich deposits of hydrothermal springs as Martian analogues, Ph.D. thesis, Univ. of Alabama at Birmingham, 1999.

Walter, M.R., and D.J. Des Marais, Preservation of biological information in thermal spring deposits: Developing **a** strategy for the search for a fossil record on Mars, *Icarus, 101,* 129-143, 1993.

Wdowiak, T.J., in *Planetary Surface Instruments Workshop,* edited by C. Meyer, A.H. Treiman, and T. Kostiuk, *LPI Tech. Rep. 95-05,* p. 94, Lunar and Planet. Inst., Houston, Tex., 1996.

Wdowiak, T.J., and D.G. Agresti, Presence of a superparamagnetic component in the Orgueil meteorite, *Nature, 311,* 140-142, 1984.

Wdowiak, T.J., D.G. Agresti, and J.D. Farmer, Mossbauer spectroscopy in the exploration for a Martian biosphere, *Eos Trans. AGU, 76*(44), Fall Meet. Suppl., F335, 1995.

Wdowiak. T.J, D.G. Agresti, S.B. Mirov, A.B. Kudryavtsev L.W. Beegle, D.J. DesMarais, and A.F. Tharpe, Identification of ancient carbonaceous cherts on Mars using Raman spectroscopy, in *Conference on Early Mars: Geologic and Hydrologic Evolution, Physical and Chemical Environments, and the Implications for Life,* edited by S.M. Clifford et **al.,** *LPI Contrib., 916,* 81-82, 1997.

Wegener, H., *Der Miissbauer Effekt und seine Anwendungen in Physik und Chemie,* 214 pp., Bibliograph. Inst., Mannheim, Germany, 1965.

Whittlesey, L.H., *Wonderland Nomenclature: A History of the Place Names of Yellowstone National Park,* 179 pp., Montana Historical Society Press, Helena, Mont., 1988.

Williams. K.P.J., J. Nelson, and **S.** Dyer, The Renishaw Raman database of gemological and mineralogical materials, *Issue* 2, 107 pp. plus Raman spectral library, Renishaw, Transducer Syst. Div., July 1997.

Woese, C.R., Bacterial evolution, *Microbiol. Rev., 51,* 221-271, 1987.

Woese, C.R., **O.** Kandler, and M.L. Wheelis, Towards a natural system of organisms: Proposal for the domains Archaea, Bacteria, and Eucarya, *Proc. Natl. Acud. Sci. U.S.A., 87,* 4576-4579, 1990.

D. G. Agresti, L. P. Armendarez, M. L. Wade, and T. J. Wdowiak, Astro and Solar System Physics Program, Department of Physics, University of Alabama at Birmingham, Birmingham. AL 35294-1170 (e-mail: agresti@uab.edu)

J. D. Farmer, Department of Geology, Arizona State University, Tempe, AZ 85287 (e-mail: jfarmer@asu.edu)

(Received August 10, 1998; revised December 11, 1998; accepted December 15, 1998.)